8-19-2022

# Cochlear ribbon synapse maturation requires Nlgn1 and Nlgn3

Miguel A Ramirez

Yuzuru Ninoyu

Cayla Miller

Leonardo R Andrade

Seby Edassery

*See next page for additional authors*

## Authors

Miguel A Ramirez, Yuzuru Ninoyu, Cayla Miller, Leonardo R Andrade, Seby Edassery, Ewa Bomba-Warczak, Briana Ortega, Uri Manor, Mark A Rutherford, Rick A Friedman, and Jeffrey N Savas

iScience

CellPress
OPEN ACCESS

Article

# Cochlear ribbon synapse maturation requires Nlgn1 and Nlgn3

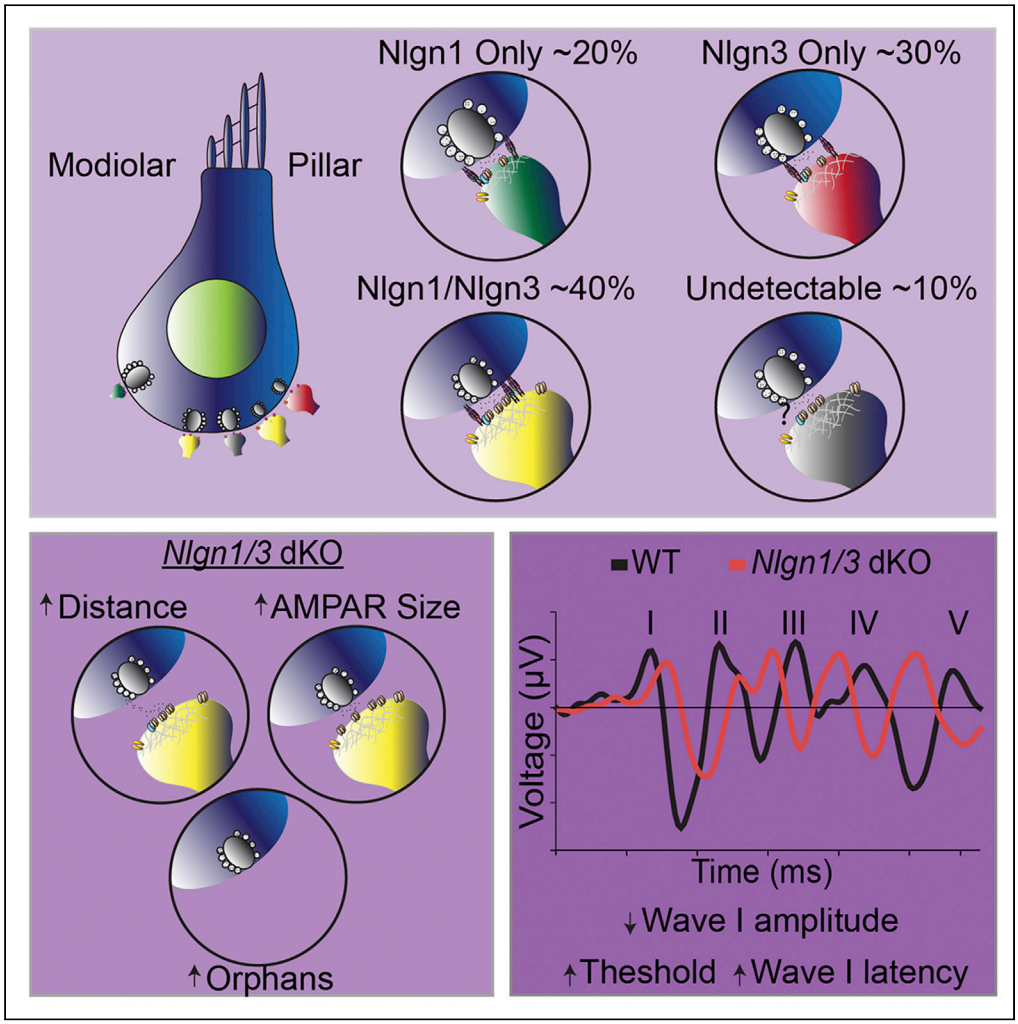


Miguel A. Ramirez, Yuzuru Ninoyu, Cayla Miller, ..., Mark A. Rutherford, Rick A. Friedman, Jeffrey N. Savas

jeffrey.savas@northwestern.edu

## Highlights

Nlgn3 is a major synapse organizing protein in spiral ganglion neurons

*Nlgn1* and *three* KO cochlea have reduced ribbon synapse density and hampered function

*Nlgn3* KO mice are highly sensitive to noise exposures

dKO cochlear phenotypes are generally synergistic and severe

Ramirez et al., iScience *25*, 104803
August 19, 2022 
https://doi.org/10.1016/j.isci.2022.104803

iScience

CellPress
OPEN ACCESS

Article

# Cochlear ribbon synapse maturation requires Nlgn1 and Nlgn3

Miguel A. Ramirez,[1] Yuzuru Ninoyu,[2] Cayla Miller,[3] Leonardo R. Andrade,[3] Seby Edassery,[1] Ewa Bomba-Warczak,[1] Briana Ortega,[2] Uri Manor,[3] Mark A. Rutherford,[4] Rick A. Friedman,[2] and Jeffrey N. Savas[1,5,*]

## SUMMARY

**Hearing depends on precise synaptic transmission between cochlear inner hair cells and spiral ganglion neurons through afferent ribbon synapses. Neuroligins (Nlgns) facilitate synapse maturation in the brain, but they have gone unstudied in the cochlea. We report *Nlgn3* and *Nlgn1* knockout (KO) cochleae have fewer ribbon synapses and have impaired hearing. *Nlgn3* KO is more vulnerable to noise trauma with limited activity at high frequencies one day after noise. Furthermore, *Nlgn3* KO cochleae have a 5-fold reduction in synapse number compared to wild type after two weeks of recovery. Double KO cochlear phenotypes are more prominent than the KOs, for example, 5-fold smaller synapses, 25% reduction in synapse density, and 30% less synaptic output. These observations indicate Nlgn3 and Nlgn1 are essential to cochlear ribbon synapse maturation and function.**

## INTRODUCTION

Hearing requires high-fidelity cochlear ribbon synapses linking mechanosensitive inner hair cells (IHCs) and spiral ganglion neuron (SGN) dendrites. The graded release of glutamate from synaptic vesicles near IHC ribbons drives synaptic transmission primarily through AMPA receptors on SGN postsynaptic terminals. Although significant progress has been made in elucidating the presynaptic release machinery and the identity of the postsynaptic glutamate receptors, very little is known about the *trans*-synaptic organizing proteins in the cochlea.

Synaptic cell adhesion proteins are critical organizers of pre- and postsynaptic proteomes. The best understood synaptic adhesion proteins are presynaptic neurexins (Nrxns) and their postsynaptic receptors the neuroligins (Nlgns). These proteins play key roles in synapse formation, specification, maturation, and function in the brain (Craig and Kang, 2007; Sudhof, 2008, 2017; Varoqueaux et al., 2006). Emerging evidence shows that Nlgn1 and Nlgn3 play partially overlapping roles in the maturation of glutamatergic synapses (Chanda et al., 2017; Shipman et al., 2011). We recently characterized the cochlear proteome and identified Nlgn3 as a predominant synaptic adhesion protein localizing to the postsynaptic membrane of ribbon synapses (Hickox et al., 2017). Moreover, *Nrxn* transcripts have been detected in transcriptomic studies of purified hair cells (Cai et al., 2015; Scheffer et al., 2015). Independently, in a pioneering large-scale mouse GWAS study, a region on chromosome 3, where the *Nlgn1* gene resides, was identified as a top candidate locus for reduced suprathreshold Wave I amplitude before and after noise trauma (Boussaty et al., 2020).

Here we report that *Nlgn3* gene expression is higher than *Nlgn1* in the cochlea during postnatal maturation. Nlgn1 and Nlgn3 primarily localize to common ribbon synapses. *Nlgn1* and *Nlgn3* single gene KOs have fewer ribbon synapses and the remaining synapses have enlarged synaptic elements which are further apart,indicative of impaired synaptic coupling. This phenotype is super-additive in mice lacking both Nlgn1 and Nlgn3, consistent with these proteins having partially redundant roles. In addition to *Nlgn1* and *Nlgn3* KO mice having compromised cochlear function and *trans*-synaptic coordination based on auditory brain stem responses (ABRs) and synapse anatomy, *Nlgn3* KOs and dKOs have impaired recovery after noise exposures from which WT mice fully recover. These results provide a pioneering description of the essential roles of Nlgn1 and Nlgn3 proteins in cochlear synapse structure and function.

[1]Department of Neurology, Feinberg School of Medicine, Northwestern University, Chicago, IL, USA

[2]Division of Otolaryngology, Department of Surgery, University of California, San Diego, 9500 Gilman Drive, Mail Code 0666, La Jolla, CA 92093, USA

[3]Waitt Advanced Biophotonics Core, Salk Institute for Biological Studies, 10010 N. Torrey Pines Road, La Jolla, CA 92037, USA

[4]Department of Otolaryngology, Washington University in St. Louis School of Medicine, St. Louis, MO, USA

[5]Lead contact

*Correspondence: jeffrey.savas@northwestern.edu

https://doi.org/10.1016/j.isci.2022.104803

## RESULTS

### Genome-wide association study analysis of hybrid mouse diversity panel identifies a significant SNP in the Nlgn1 loci

A functional screen aimed to identify genetic loci associated with deviations in suprathreshold Wave I in hybrid mouse diversity panel (HMDP) strains were previously reported and identified a region on chromosome 3 as a locus of interest (Boussaty et al., 2020; Lusis et al., 2016). This experiment considered 102 different mouse strains and performed a total of 635 ABR recordings to elucidate changes in cochlear output among the HMDP mice. A careful re-analysis of genome-wide association study (GWAS) results for ABR Wave I amplitudes at four frequencies (8, 16, 24, 32 kHz) identified a small panel of notable loci. There were no significant associations related to the changes in Wave I amplitude in response to eight or 32 kHz tone burst stimulation. At 16 kHz there was a single expression quantitative trait locus containing the *Robo1* gene as previously reported (Boussaty et al., 2020). At 24 kHz, we identified a single locus on chromosome three was near the *Nlgn1* gene (Figure S1A). A higher resolution assessment of the significant single-nucleotide polymorphism localized to the 25.5–26.0 Mb region of chromosome three which contains the *Nlgn1* gene (Figure S1B). Targeted examination of the 101.1–101.5 Mb region on chromosome 23 (i.e. X), which contains the *Nlgn3* gene revealed only two loci, both of which failed to reach significance (Figure S1C).

### Neuroligins are primarily expressed by cochlear spiral ganglion neurons and not hair cells

We first determined which cells within the cochlea express neuroligins. Given that the IHC-SGN afferent ribbon synapses are glutamatergic, we focused our investigation on Nlgn1 and Nlgn3, which both localize to postsynaptic membranes of excitatory synapses (Budreck and Scheiffele, 2007; Scheiffele et al., 2000; Song et al., 1999). To visualize the expression of *Nlgn1* and *Nlgn3* within the spiral ganglion and organ of Corti we used multiplexed RNAScope *in situ* hybridization (ISH) in 12 μm thick mid-modiolar radial sections at P60. We detected *Nlgn1* and *Nlgn3* expression predominantly in SGNs based on overlap with *Tubb1* (i.e. *β-tub*) but not *MyosinVIIa* (i.e. *Myo7a*), markers for SGNs and hair cells, respectively (Figures 1A and 1B). Each SGN innervates a single IHC, therefore, determining the proportion of SGNs expressing either *Nlgn1* and/or *Nlgn3* will provide insight into the combination of neuroligins present at IHC ribbon synapses (Meyer et al., 2009).

Having determined that SGNs express *Nlgn1 and Nlgn3,* we next sought to investigate the proportion of SGNs which express either *Nlgn1* and/or *Nlgn3*. Within the mid-modiolar section all three regions of the cochlea (i.e. apical (4–12 kHz), middle (12–32 kHz), and basal (32–64 kHz) can be visualized. Analysis of the neuroligin expression revealed no obvious tonotopic gradient with 86 ± 5.1% of cells expressing *Nlgn1* and 85 ± 5.3% of cells expressing *Nlgn3* throughout the turns of the cochlea (Figures S1D and S1E). Moreover, 72 ± 10.4% of all cells within the bundle were positive for both *Nlgn1* and *Nlgn3,* suggesting that *Nlgn1* and *Nlgn3* are expressed by many of the same neurons throughout the cochlea.

### Nlgn1 and Nlgn3 localize to common and distinct ribbon synapses

To confirm Nlgn1 and Nlgn3 proteins localize to ribbon synapses to a similar degree as expected based on the RNAScope ISH data, we used immunofluorescence (IF) and confocal microscopy analysis of cochlear explants. To ensure the specificity of the neuroligin antibodies we obtained *Nlgn1* KO and *Nlgn3* KO mice (Varoqueaux et al., 2006), and performed Western blot (WB) and IF analysis of cochlear explants (Figures 2A, 2D, and S2A). We visualized Nlgn1 puncta relative to ribbon synapses based on C-terminal binding protein 2 (CtBP2) in IHCs juxtaposed to GluA2 in SGNs in KO and WT mice (Figure 2B). Nlgn1 was present at about two-thirds of ribbon synapses (68 ± 2.1%) (Figure 2C). Parallel IF analysis of Nlgn3 revealed that a slightly larger proportion of ribbon synapses contain Nlgn3 (77 ± 2.6%) (Figures 2E and 2F). Additionally, we confirmed that Nlgn2 was not present among the cochlear ribbon synapses and that both Nlgn1 and Nlgn3 were also present among outer hair cells in addition to the presence of Nrxns among ribbon synapses (Figures S2B–S2D). To investigate whether neuroligins localize to cochlear ribbon synapses in other species, we confirmed synaptic localization with additional IF experiments in rat and marmoset cochlear whole mounts (Figures S2E and S2F).

Next, we determined whether Nlgn1 and Nlgn3 are present at common or distinct cochlear ribbon synapses. We found that 40 ± 6.7% of synapses contain both Nlgn1 and Nlgn3, 17 ± 9.5% were positive for only Nlgn1, and 31 ± 4.2% only for Nlgn3, while 11 ± 8.1% had undetectable levels for both neuroligins

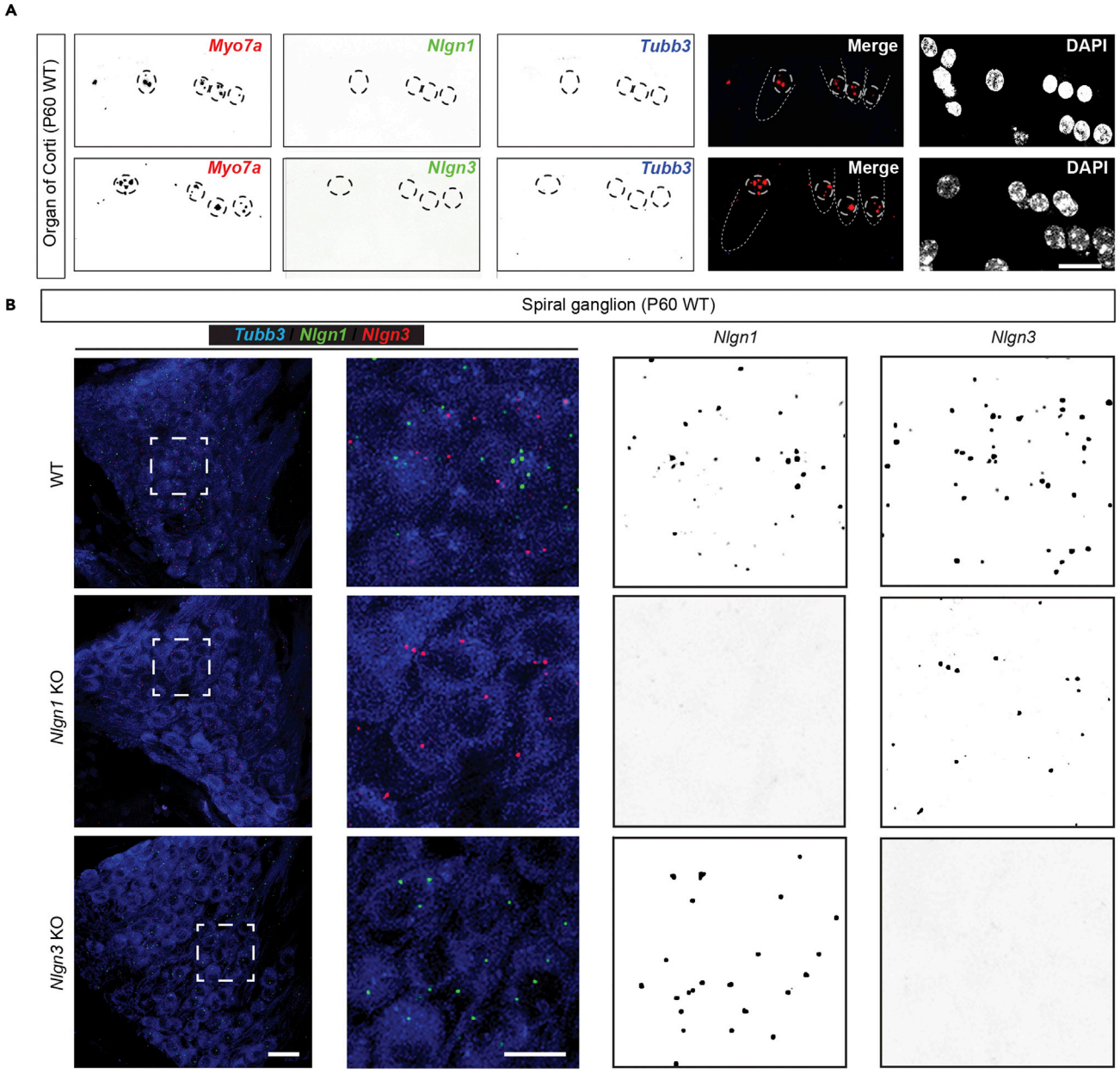


**Figure 1. *Nlgn1* and *Nlgn3* are predominantly expressed by spiral ganglion neurons**

(A) Representative fluorescent images from RNAScope *in situ* hybridization analysis from Organ of Corti sections. Top: *Nlgn1* (green); Bottom: *Nlgn3* (green), expression was undetectable in cells positive for *Myo7a* (red) and *Tubb3* (blue).

(B) Representative fluorescent images from RNAScope *in situ* hybridization analysis from 12 μm-thick sections of spiral ganglion in WT, *Nlgn1* KO, or *Nlgn3* KO cochlea. *Nlgn1* (green) and *Nlgn3* (red) expression was detectable in cells positive for *Tubb3* (blue). Probe specificity was validated in KO tissues which demonstrate little to no reactivity for *Nlgn1* or *Nlgn3* probes.

Scale bar = 10 μm (A and B). Mice were aged P60-65 per genotype.

(Figures 2G and 2H). The presence of synapses that lack either Nlgn1 or Nlgn3 is of particular interest as this potentially lends itself toward distinct roles for these proteins within the cochlea. Recently there has been growing interest in the characterization of IHC-ANF synapse subtypes, which broadly are divided into three categories (Liberman, 1982; Shrestha et al., 2018; Sun et al., 2018). The type Ia-Ic SGNs are theorized to have somewhat spatially segregated innervation patterns along the pillar to modiolar inner hair cell axis that is closely linked to their activity patterns. Generally, the type Ib fibers innervate regions closer to

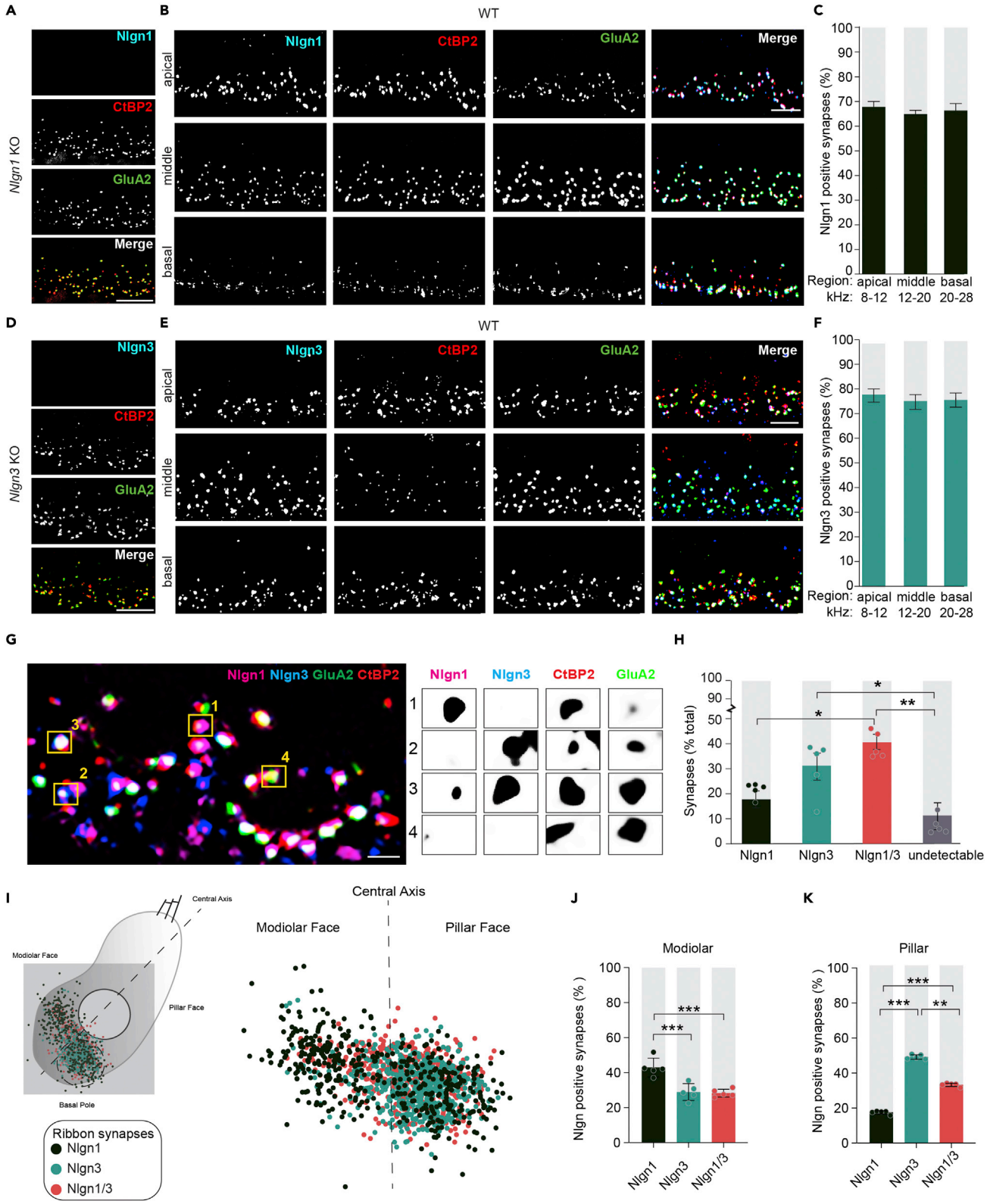
A
B
WT
C
Nlgn1
CtBP2
GluA2
Merge
Nlgn1 KO
apical
middle
basal
Nlgn1 positive synapses (%)
Region: apical middle basal
kHz: 8-12 12-20 20-28
D
E
WT
F
Nlgn3
Nlgn3 KO
Nlgn3 positive synapses (%)
G
Nlgn1 Nlgn3 GluA2 CtBP2
H
Synapses (% total)
Nlgn1
Nlgn3
Nlgn1/3
undetectable
I
Central Axis
Modiolar Face
Pillar Face
Basal Pole
Ribbon synapses
Nlgn1
Nlgn3
Nlgn1/3
J
Modiolar
Nlgn positive synapses (% )
K
Pillar

**Figure 2. Nlgn1 and Nlgn3 are present at cochlear ribbon synapses in a modiolar-pillar position dependent pattern**

(A) Representative immunofluorescent images from *Nlgn1* KO cochlear whole mounts demonstrating the absence of Nlgn1 at ribbon synapse (CtBP2 = red, GluA2 = green).

(B) Representative images from apical (8–12 kHz), middle (12–20 kHz), and basal (20–28 kHz) regions of the cochlea immunostained with antibodies for Nlgn1 (blue) and IHC ribbon synapse markers CtBP2 (red) and GluA2 (green).

(C) Quantification of (B) reveals that on average Nlgn1 is present at greater than 65% of all IHC ribbon synapses within the cochlea.

(D) Representative immunofluorescent images from *Nlgn3* KO cochlear whole mounts demonstrating the absence of Nlgn3 at ribbon synapse (CtBP2 = red, GluA2 = green).

(E) Representative images from apical (8–12 kHz), middle (12–20 kHz), and basal (20–28 kHz) regions of the cochlea immunostained with antibodies for Nlgn3 (blue), CtBP2 (red), and GluA2 (green).

(F) Quantification of (E) reveals that on average Nlgn3 is present at greater than 78% of inner hair cell ribbon synapses within the cochlea.

(G) Representative images of ribbon synapses immunostained with antibodies for Nlgn1 (magenta), Nlgn3 (blue), CtBP2 (red), and GluA2 (green); subpanels one to four are enlargements of four individual synapses. Data from 16 to 20 kHz region of the cochlea.

(H) Quantification of (G) revealed that 40 $\pm$ 6.7% of all ribbon synapses contain both Nlgn1 and 3, 17 $\pm$ 9.5% were positive for only Nlgn1, 31 $\pm$ 4.2% were positive for only Nlgn3, and 11 $\pm$ 8.1% of ribbon synapses had undetectable levels of either Nlgn1 or 3 (n = 1306 synapses).

(I) Nlgn1 and Nlgn3 positive synapse coordinates plotted according to the IHC pillar-to-modiolar axis from the 16–20 kHz region of the cochlea. Dotted lines represent the basal pole and the line demarcating the pillar to modiolar boarder used for analysis.

(J) Quantification of (I) reveals that on the modiolar side a larger proportion of ribbon synapses contained exclusively Nlgn1 (42 $\pm$ 5.4%) compared to exclusively Nlgn3 (29 $\pm$ 4.8).

(K) Quantification of (I) revealed that on the pillar face the majority of synapses were populated with Nlgn3 (Nlgn1 exclusive: 18 $\pm$ 5.4%, Nlgn3 exclusive: 49 $\pm$ 1.3%, and Nlgn1 and Nlgn3: 33 $\pm$ 1.0%).

Data are represented as mean $\pm$ SD. * = p value <0.05, ** = p value <0.01, *** = p value <0.001 by one-way ANOVA with Tukey post hoc correction for pairwise comparison. Scale bar = 10 μm (A, B, D, and E), 2 μm (G). N = 5 mice per genotype aged P60-65.

the modiolar face of inner hair cells and are believed to have higher thresholds compared to the type Ia and Ic fibers that localize to the pillar face (Furman et al., 2013; Liberman, 1982; Petitpre et al., 2018; Shrestha et al., 2018). Thus, to investigate the possibility that Nlgn1 and Nlgn3 have distinct roles among the subtypes of ribbon synapses, we quantified synapses containing either Nlgn1 or Nlgn3 or both across the pillar to modiolar axis of inner hair cell from the 16–20 kHz region of the cochlea (Figures 2I and S2G). A larger proportion of Nlgn1 exclusive synapses (43 $\pm$ 5.4%) were present on the modiolar face compared to Nlgn3 exclusive (29 $\pm$ 4.8%) synapses (Figure 2J). Conversely, on the pillar face the opposite was found, most synapses were populated with Nlgn3 (Nlgn1 exclusive: 18 $\pm$ 0.51%, Nlgn3 exclusive: 49 $\pm$ 1.3%, and Nlgn1 and Nlgn3: 33 $\pm$ 1.0%) (Figure 2K). Consistent with our findings, two labs have independently published databases that determined that *Nlgn3* is expressed to a similar degree among type Ia, Ib, and Ic, whereas *Nlgn1* was seen to be lowly expressed among type Ib SGNs (Petitpre et al., 2018; Shrestha et al., 2018). Together demonstrates that in addition to potentially overlapping roles for Nlgn1 and Nlgn3 at the same synapses, there exists a pool of synapses along the pillar-modiolar axis where Nlgn1 and Nlgn3 may play more distinct roles.

## Ribbon synapses are significantly fewer and smaller in Nlgn1/3 double KO mice

To investigate if Nlgn1 or Nlgn3 are required for ribbon synapse maintenance we performed IF analysis of cochlear whole mounts from *Nlgn1* KO, *Nlgn3* KO, and *Nlgn1/3* dKO mice (Figures 3A–3D). Across the base, middle, and apical regions of the cochlea, loss of Nlgn1 or Nlgn3 resulted in about a 10% reduction in synapse density (*Nlgn1* KO: 92 $\pm$ 2.4%, *Nlgn3* KO: 93 $\pm$ 3.8%). Markedly, the dKO mice had a more pronounced 25% reduction in ribbon synapse density compared to WT (*Nlgn1/3* dKO: 76 $\pm$ 2.2%) (Figure 3E). We then quantified the number of orphan ribbons (i.e. CtBP2 puncta without colocalized GluA2 puncta) in KO and dKO cochleae relative to WT controls. Notably, *Nlgn1* KO mice had a significantly greater number of orphan ribbons compared to WT or *Nlgn3* KO mice (*Nlgn1* KO: 1.4 $\pm$ 0.61, *Nlgn3* KO: 0.31 $\pm$ 0.10, WT: 0.30 $\pm$ 0.20 orphans per inner hair cell) (Figure 3F). Strikingly, mice lacking both Nlgn1 and three had a dramatic increase in the number of orphan ribbons, (*Nlgn1/3* dKO: 5.7 $\pm$ 1.5 orphans per inner hair cell), suggesting that Nlgn1 has a more prominent role in physically linking pre- and postsynaptic elements in the cochlea.

We next measured the extent of spatial overlap between CtBP2 and GluA2 for each individual synapse (hereafter referred to simply as "synapse volume") across each genotype and found a significant ~50% decrease in *Nlgn1* and *Nlgn3* KOs compared to WT. The absence of both neuroligins resulted in greater than a 5-fold reduction in ribbon synapse volume (Figure 3G). To further investigate this finding, we then asked if this reduction in volume was owing to smaller AMPARs clusters or ribbons. Notably, we found that the absence of Nlgn1 and Nlgn3 resulted in enlarged GluA2 puncta volume (Figure S3A). We also

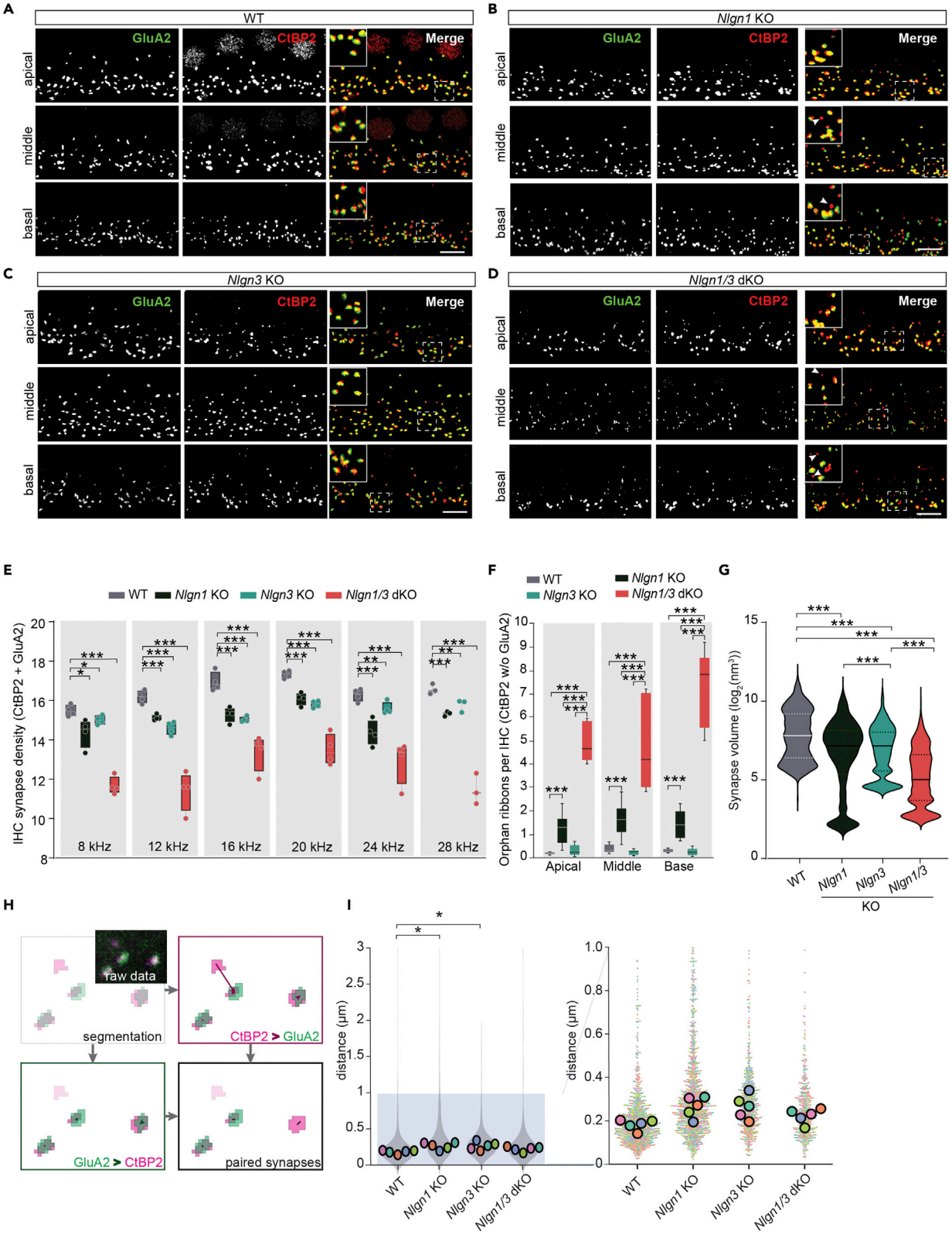
A
WT
GluA2
CtBP2
Merge
apical
middle
basal
B
Nlgn1 KO
C
Nlgn3 KO
D
Nlgn1/3 dKO
E
WT
Nlgn1 KO
Nlgn3 KO
Nlgn1/3 dKO
IHC synapse density (CtBP2 + GluA2)
8 kHz
12 kHz
16 kHz
20 kHz
24 kHz
28 kHz
F
Orphan ribbons per IHC (CtBP2 w/o GluA2)
Apical
Middle
Base
G
Synapse volume (log2(nm3))
WT
Nlgn1
Nlgn3
Nlgn1/3
KO
H
raw data
segmentation
CtBP2 > GluA2
GluA2 > CtBP2
paired synapses
I
distance (µm)
WT
Nlgn1 KO
Nlgn3 KO
Nlgn1/3 dKO

**Figure 3. Nlgn1 and three are required for cochlear ribbon synapse maturation**

(A–D) Representative images from WT, *Nlgn1* KO, *Nlgn3* KO and *Nlgn1/3* dKO cochlear wholemounts from P60-65 mice immunostained with the indicated antibodies for ribbon synapses. Instances of orphan ribbons are marketed by arrows.

(E) Synaptic density was significantly reduced at all measured regions: 8 kHz: WT 15.5 ± 0.28, *Nlgn1* KO 14.4 ± 0.72, *Nlgn3* KO 15 ± 0.22, *Nlgn1/3* dKO 11.7 ± 0.45; 12 kHz: WT 16.2 ± 0.32, *Nlgn1* KO 15.1 ± 0.14, *Nlgn3* KO 14.6 ± 0.33, *Nlgn1/3* dKO 11.4 ± 1.0; 16 kHz: WT 17.0 ± 0.49, *Nlgn1* KO 15.3 ± 0.37, *Nlgn3* KO 15 ± 0.13, *Nlgn1/3* dKO 13.3 ± 0.93; 20 kHz: WT 17.3 ± 0.19, *Nlgn1* KO 16 ± 0.31, *Nlgn3* KO 15.8 ± 0.17, *Nlgn1/3* dKO 13.5 ± 0.79; 24 kHz: WT 16.6 ± 0.26, *Nlgn1* KO 15.3 ± 0.12, *Nlgn3* KO 15.8 ± 0.32, *Nlgn1/3* dKO 11.6 ± 0.79; 28 kHz: WT 16.5 ± 0.64, *Nlgn1* KO 15.1 ± 0.66, *Nlgn3* KO 15.3 ± 0.5, *Nlgn1/3* dKO 12.4 ± 0.98.

(F) The number of orphan ribbons per IHC was elevated in both *Nlgn1* KO and dKO mice compared to WT in the apical (WT: 0.23 ± 0.04; *Nlgn1* KO: 1.2 ± 0.61; *Nlgn1/3* dKO: 4.9 ± 0.85), middle (WT: 0.41 ± 0.16; *Nlgn1* KO: 1.7 ± 0.69; *Nlgn1/3* dKO: 4.8 ± 2.0) and basal (WT: 0.31 ± 0.09; *Nlgn1* KO: 1.5 ± 0.54; *Nlgn1/3* dKO: 7.2 ± 1.6) regions of the cochlea. Box and whisker plot highlighting the 25th-75th quartile distribution middle line is the median of the distribution.

(G) Single gene KO cochlea had significantly reduced afferent synapse volume, on average, compared to WT (*Nlgn1* KO: 0.21 ± 0.05 $\mu m^3$, *Nlgn3* KO: 0.19 ± 0.04 $\mu m^3$, WT: 0.40 ± 0.19 $\mu m^3$). Analysis of the *Nlgn1/3* dKO cochlea reveal an exacerbated phenotype (0.07 ± 0.01 $\mu m^3$).

(H) Schematic representation of how distances between pre- and postsynaptic elements were measured to identify nearest neighbors. Distances were measured from the center of each CtBP2 punctum to its nearest neighboring GluA2 punctum to generate a list of nearest neighbors from CtBP2, and vice versa. Lists were then compared to keep only the closest pairs common to both lists, thus eliminating mismatched lone puncta.

(I) The average distance between presynaptic CtBP2 and postsynaptic GluA2 is enhanced in *Nlgn1* KO cochlea (0.26 ± 0.05 μm) and *Nlgn3* KO cochlea (0.26 ± 0.06 μm) compared to WT (0.18 ± 0.02 μm) and *Nlgn1/3* dKO (0.21 ± 0.03 μm) cochlea.

Data are represented as mean ± SD. * = p value <0.05, ** = p value <0.01, *** = p value <0.001 by one-way ANOVA with Tukey post hoc correction. Scale bar = 10 μm (A–D), N = 4 (A–E), 8 (F), 5 (G–I) P60-65 mice per genotype.

found that the ribbons were significantly larger among *Nlgn1* and *Nlgn1/3* dKO inner hair cells (Figure S3B). At odds with reduced synaptic volumes, it was curious that both pre- and postsynaptic elements are enlarged across the single and double KOs. To address this disparity, we next determined whether the distance between paired CtBP2 and GluA2 puncta was greater (Figure 3H). Indeed, the average distance between these pre and postsynaptic markers was significantly greater in *Nlgn1,* and *Nlgn3* KO cochlea compared to WT (Figure 3I). To further investigate how synaptic architecture may be altered in the absence of both Nlgn1 and Nlgn3 we performed transmission electron microscopy. Indeed, the distance between pre and post-synaptic membranes (i.e. synaptic cleft) of the cochlear ribbon synapses was enlarged in the *Nlgn1/3* dKO synapses (18 ± 8.8 nm) compared to WT synapses (12 ± 2.8 nm) (Figure S3C). Consistent with previous findings showing that over-expression of a dominant negative form of Nlgn1 can drive the misalignment of AMPAR nanoclusters and release sites in cultured neurons (Haas et al., 2018). We independently confirmed that Nlgn1 is required for proper alignment of cochlear pre- and postsynaptic elements in Pax2-Cre; $Nlgn1^{fl/fl}$ (i.e. *Nlgn1* cKO) (Figures S3E and S3F), suggesting that the reduced volumes recorded in the single KOs are a result of an increase in the distance of the pre- and postsynaptic elements despite the enlargement of AMPAR and ribbon puncta volumes.

To delineate whether reduced synaptic density resulted from impaired formation during the development or maturation of ribbon synapses, we quantified *Nlgn1, 2,* and *three* gene expression and synapse density at major milestones in cochlear maturation such as the onset of hearing at P12 (Takahashi et al., 2018). Although previous research has detected neuroligin expression in the cochlea, little is known regarding the patterns of expression throughout postnatal cochlear maturation (Petitpre et al., 2018; Shrestha et al., 2018). Thus, we compared *Nlgn1, 2, three* mRNA levels at P1 (postnatal day 1), P6, P12, and P30 (Figure S3G). *Nlgn1* and *Nlgn2* mRNA levels are highest at P1. In contrast, *Nlgn3* expression progressively increased throughout maturation (*Nlgn3*: P1 = 0.43 ± 0.05, P6 = 1.45 ± 0.05, P12 = 2.27 ± 0.04, P30 = 2.97 ± 0.06). To determine if synapse density is reduced before the onset of hearing (i.e. P12) we analyzed cochlea from P12 and P30 in single and double KO compared to WT (Figure S3G). Synapse density at P12 was similar in *Nlgn1* and *Nlgn3* KOs and dKOs compared to WT mice (Figure S3H). However, synaptic density was significantly reduced among neuroligin KOs and dKOs at P30 compared to WT mice (*Nlgn1* KO: 15 ± 0.9, *Nlgn3* KO: 14 ± 1.2, *Nlgn1/3* dKO: 13 ± 0.46, WT 16 ± 0.7 synapses per IHC). Together this suggests that the reduction in synaptic density observed in the adult cochlea in neuroligin KOs is the result of an impairment in the maturation of synapses after the onset of hearing rather than a failure in synapse formation pre-hearing.

## Absence of Nlgn1 or Nlgn3 impairs hearing

To assess the functional role of Nlgn1 or Nlgn3 in hearing we performed auditory brainstem response (ABR) hearing measurements (Figure 4A). ABR recordings are sound-evoked field potentials recorded from the ascending auditory pathway in response to sound. Comparison of ABR thresholds (i.e. the minimum

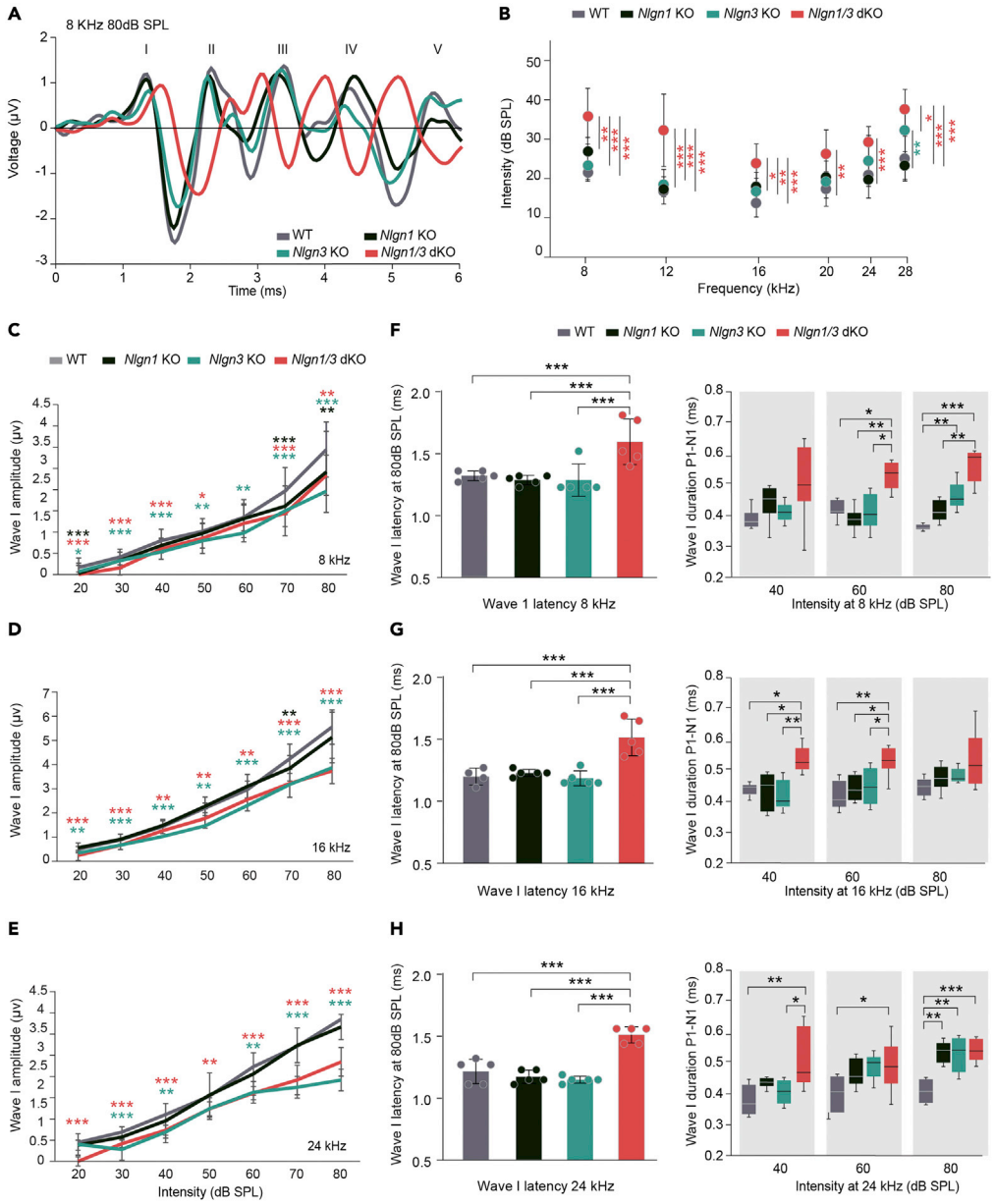


**Figure 4. Nlgn1 and three are required for cochlear function**

(A) Representative ABR waveforms at 8 kHz and 80 dB SPL by genotype. Wave-I amplitude was measured peak to trough; latency was measured from sound onset to P1; duration was measured as time from P1 to N1.

(B) Quantification reveals ABR thresholds were largely unaffected in either *Nlgn1* or *Nlgn3* KOs compared to WT. *Nlgn3* KOs had elevated threshold levels only at 28 kHz (WT: 25 ± 6.0 dB SPL, *Nlgn3* KO: 33 ± 6.6 dB SPL). *Nlgn1/3* dKO mice had significantly elevated thresholds at all tested frequencies.

(C–E) Growth response curves for 8, 16, and 24 kHz from 20 to 80 dB SPL show significant reduction in ABR responses predominantly between *Nlgn3* KO and *Nlgn1/3* dKOs compared to WT. Wave I amplitude at 8 kHz 80 dB SPL: WT 3.6 ± 0.31 μV, *Nlgn1* KO 2.9 ± 0.66 μV, *Nlgn3* KO 2.2 ± 0.45 μV, *Nlgn1/3* dKO 2.71 ± 0.73 μV. Wave I amplitude at 16 kHz 80 dB SPL: WT 6.0 ± 0.58 μV, *Nlgn1* KO 5.4 ± 1.01 μV, *Nlgn3* KO 3.9 ± 0.25 μV, *Nlgn1/3* dKO 3.8 ± 0.53 μV. Wave I amplitude at 24 kHz 80 dB SPL: WT 3.7 ± 0.38 μV, *Nlgn1* KO 3.5 ± 0.55 μV, *Nlgn3* KO 2.1 ± 0.33 μV, *Nlgn1/3* dKO 2.6 ± 0.43 μV.

(F–H) Wave-I latency was significantly increased in dKO mice compared to *Nlgn1* KO, *Nlgn3* KO, or WT mice (8 kHz: *Nlgn1/3* dKO: 1.6 ± 0.18 ms, WT: 1.3 ± 0.04 ms, *Nlgn1* KO: 1.3 ± 0.13 ms, *Nlgn3* KO: 1.3 ± 0.13 ms; 16 kHz: *Nlgn1/3* dKO: 1.5 ± 0.15 ms, WT: 1.2 ± 0.07 ms, *Nlgn1* KO: 1.2 ± 0.03 ms, *Nlgn3* KO: 1.2 ± 0.06 ms; 24 kHz: *Nlgn1/3* dKO: 1.5 ± 0.05 ms, WT: 1.2 ± 0.10 ms, *Nlgn1* KO: 1.2 ± 0.05 ms, *Nlgn3* KO: 1.2 ± 0.03 ms). The duration of Wave I was significantly increased in *Nlgn1/3* dKO mice compared to WT at higher intensities at 8 kHz: (40 dB: WT 0.4 ± 0.03 ms, *Nlgn1* KO

**Figure 4. *Continued***

0.43 ± 0.07 ms, *Nlgn3* KO 0.41 ± 0.03 ms, *Nlgn1/3* dKO 0.50 ± 0.14 ms; 80 dB: WT 0.37 ± 0.01 ms, *Nlgn1* KO 0.42 ± 0.04 ms, *Nlgn3* KO 0.47 ± 0.05 ms, *Nlgn1/3* dKO 0.53 ± 0.14 ms), 16 kHz: (40 dB: WT 0.44 ± 0.02 ms, *Nlgn1* KO 0.44 ± 0.04 ms, *Nlgn3* KO 0.43 ± 0.05 ms, *Nlgn1/3* dKO 0.54 ± 0.04 ms; 80 dB: WT 0.45 ± 0.02 ms, *Nlgn1* KO 0.49 ± 0.04 ms, *Nlgn3* KO 0.45 ± 0.05 ms, *Nlgn1/3* dKO 0.52 ± 0.06 ms) and 24 kHz: (40 dB: WT 0.38 ± 0.05 ms, *Nlgn1* KO 0.44 ± 0.02 ms, *Nlgn3* KO 0.42 ± 0.04 ms, *Nlgn1/3* dKO 0.51 ± 0.11 ms; 80 dB: WT 0.41 ± 0.04 ms, *Nlgn1* KO 0.53 ± 0.03 ms, *Nlgn3* KO 0.53 ± 0.06 ms, *Nlgn1/3* dKO 0.56 ± 0.03 ms).

Data are represented as mean ± SD. * = p value <0.05, ** = p value <0.01, *** = p value <0.001 by one-way ANOVA with Tukey post hoc correction. N = 8 mice for (A–C), five mice for (D–H) at P60-65 per genotype

auditory stimuli needed to evoke an ABR response above the noise floor of 0.18 μv) in WT littermates of *Nlgn1* and *Nlgn3* single KOs demonstrated no significant differences across the background strains (Figures S4A and S4B). Distortion product otoacoustic emissions in *Nlgn1* KOs, *Nlgn3* KOs, and *Nlgn1/3* dKOs were similar to WT, suggesting that outer hair cell function is unaffected (Figure S4C). ABR responses from *Nlgn3* KOs displayed a significant elevation in threshold only at 28 kHz compared to WT (Figure 4B). In contrast, *Nlgn1/3* dKOs had robustly elevated threshold levels, which on average were 12 ± 3.0 dB higher than both WT and single KOs at all tested frequencies. Next, we assessed Wave I amplitude, which reflects the number of activated SGNs at increasing levels of sound stimulation. *Nlgn1* KO had significantly reduced Wave I amplitude at 8 kHz with 80 dB of sound pressure level (dB SPL) stimuli compared to WT (Figure 4C). *Nlgn3* KO and *Nlgn1/3* dKOs Wave I amplitudes at 80 dB SPL were significantly reduced by 31 ± 12% and 32 ± 14%, respectively across all frequencies compared to WT (Figures 4C–4E). Wave I amplitudes were significantly reduced at most tested intensities for *Nlgn3,* and *Nlgn1/3* (d)KOs compare to WT, suggesting a global decrease in neuronal activity. To follow-up on the cochlear phenotypes observed, we next investigated response latencies. ABR analysis of the 8, 16, and 24 kHz revealed an increased duration and onset-latency of Wave I at both 60- and 80-dB SPL stimuli in dKOs compared to WT (Figures 4F–4H). Given the absence of a robust reduction in Wave I amplitude phenotype among *Nlgn1* KO mice, we investigated the possibility of compensatory *Nlgn3* gene expression. We found that Nlgn3 gene expression was, indeed, upregulated in *Nlgn1* KO cochlea while Nlgn1 expression was comparable to WT in *Nlgn3* KO cochlea (Figure S4D). Utilizing IF, we independently confirmed compensatory Nlgn3 synaptic expression at *Nlgn1* KO cochlea ribbon synapses (Figure S4E). Together suggests that the mild hearing phenotype observed in *Nlgn1* KO mice may be mitigated in part by Nlgn3 compensation. Independent investigation of ABR responses from *Nlgn1* cKO revealed the presence of a latency effect, further supporting the possibility of potential compensation by Nlgn3 in *Nlgn1* KO mice (Figure S4F).

## Mice lacking Nlgn1 or Nlgn3 are highly sensitive to loud noise

Given that neuroligins function as *trans*-synaptic adhesion proteins, we hypothesized that *Nlgn1* or *Nlgn3* KO cochlea would be more sensitive to acoustic trauma compared to WT controls. Young adult mice were exposed to band-pass filtered white noise (6–18 kHz) for 30 min at 94 dB SPL (Jongkamonwiwat et al., 2020). ABRs were measured before and 1, 7, and 14 days after noise exposure (DAN). As expected, this noise insult resulted in a significant threshold shift of ~20–30 dB at 16 and 24 kHz but only a 2 dB shift at 8 kHz one DAN in WT mice. However, at 14 DAN ABR thresholds fully recovered to pre-noise exposure levels at 8, 16, and 24 kHz (Figure 5A). We found no significant differences between the background strains with respect to noise sensitivity or recovery from noise two weeks following exposure (Figures S5A and S5B). Both single and double KOs had significant threshold shifts 1DAN compared to WT at 8 kHz (Figures 5A–5D). Strikingly, *Nlgn3* KOs failed to generate a Wave I response at 80 dB SPL above 24 kHz and on average exhibited a 43 ± 12 dB shift at 16 kHz (Figures 5C and S5C). At 14 DAN *Nlgn1* KO thresholds fully recovered with a non-significant 6.7 ± 5.1 dB residual shift (Figure S5C). *Nlgn3* KOs had only a very limited recovery at 24 kHz 14 DAN with an average threshold shift of 29 ± 17 dB *Nlgn1/3 dKO* had significantly elevated thresholds beginning one DAN at 8, 16, and 24 kHz, and only demonstrated recovery at 8 kHz (Figures 5D and S5C).

To determine if cochleae lacking Nlgn1 or Nlgn3 have hampered Wave I amplitudes 14 DAN relative to before noise. Comparison of Wave I amplitudes (80 dB SPL stimuli) relative to before noise revealed a gradual recovery of cochlear output in WT mice, which largely recovered to baseline levels 14 DAN at 8, 16, and 24 kHz (Figure 5E). For *Nlgn1* KO, the only frequency range that failed to fully recover was 8 kHz which on average had a 22 ± 11% reduction in synaptic strength compared to before noise (Figure 5F). Consistent with the dramatic threshold shifts observed in *Nlgn3* KO and *Nlgn1/3* dKO mice, Wave I amplitudes failed to recover at 16 and 24 kHz even 14 DAN, while at 8 kHz amplitudes fully recovered for *Nlgn3 KOs but not Nlgn1/3* dKOs (Figures 5G and 5H). Next, we performed IF analysis across the 20–24 kHz region

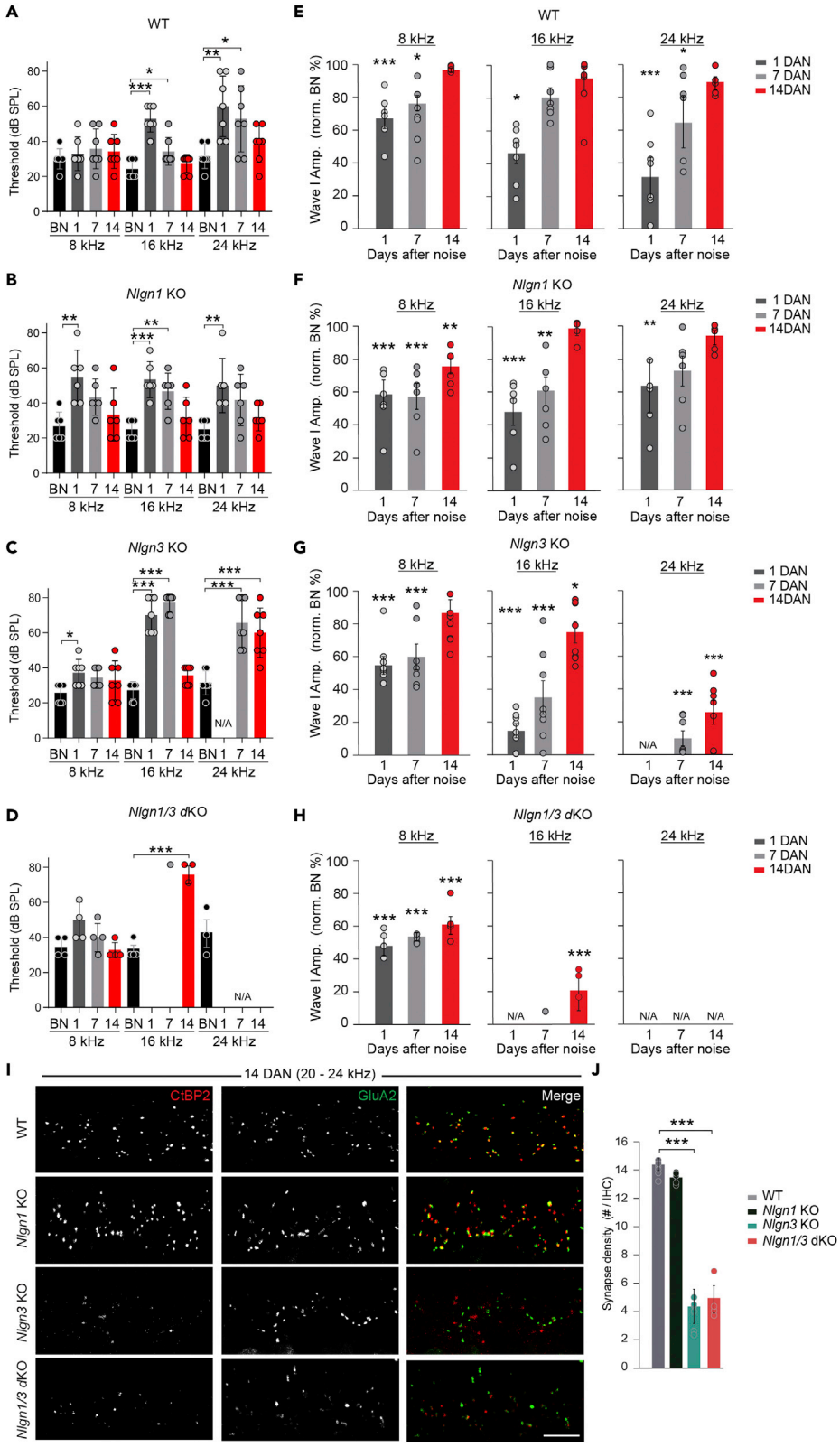
A
WT
Threshold (dB SPL)
BN 1 7 14 BN 1 7 14 BN 1 7 14
8 kHz
16 kHz
24 kHz
E
WT
8 kHz
16 kHz
24 kHz
Wave I Amp. (norm. BN %)
Days after noise
1 DAN
7 DAN
14DAN
B
Nlgn1 KO
F
Nlgn1 KO
C
Nlgn3 KO
G
Nlgn3 KO
D
Nlgn1/3 dKO
H
Nlgn1/3 dKO
N/A
I
14 DAN (20 - 24 kHz)
CtBP2
GluA2
Merge
WT
Nlgn1 KO
Nlgn3 KO
Nlgn1/3 dKO
J
Synapse density (# / IHC)
WT
Nlgn1 KO
Nlgn3 KO
Nlgn1/3 dKO

**Figure 5. *Nlgn3* KOs have increased sensitivity to noise**

(A) In WT mice ABR thresholds fully recovered to before noise (BN) threshold levels by 14 DAN at 8 kHz (BN = 30 ± 5.8 dB SPL, one DAN = 33 ± 9.5 dB SPL, seven DAN = 36 ± 11 dB SPL, 14 DAN = 34 ± 9.8 dB SPL), 16 kHz (BN = 24 ± 5.3 dB SPL, one DAN = 52 ± 7.5 dB SPL, seven DAN = 34 ± 7.9 dB SPL, 14 DAN = 27 ± 4.8 dB SPL), and 24 kHz (BN = 31 ± 6.8 dB SPL, one DAN = 60 ± 17.3 dB SPL, seven DAN = 52 ± 18.9 dB SPL, 14 DAN = 38 ± 10.7 dB SPL) after 30 min exposure to 94 dB SPL.

(B) In *Nlgn1* KO mice ABR thresholds fully recovered to BN threshold levels by 14 DAN at 8 kHz (BN = 26 ± 8.16 dB SPL, one DAN = 55 ± 15.2 dB SPL, seven DAN = 43 ± 10.3 dB SPL, 14 DAN = 32 ± 15.0 dB SPL), 16 kHz (BN = 25 ± 5.47 dB SPL, one DAN = 53 ± 10.3 dB SPL, seven DAN = 47 ± 10.3 dB SPL, 14 DAN = 32 ± 7.5 dB SPL), and 24 kHz (BN = 25 ± 5.47 dB SPL, one DAN = 50 ± 15.5 dB SPL, seven DAN = 42 ± 14.7 dB SPL, 14 DAN = 31 ± 7.5 dB SPL).

(C) In *Nlgn3* KO mice ABR thresholds fully recovered to BN threshold levels by 14 DAN at 8 kHz (BN = 27 ± 4.9 dB SPL, one DAN = 56 ± 16 dB SPL, seven DAN = 34 ± 5.3 dB SPL, 14 DAN = 60 ± 11 dB SPL) and 16 kHz (BN = 27 ± 4.9 dB SPL, one DAN = 70 ± 10.0 dB SPL, seven DAN = 66 ± 14 dB SPL, 14 DAN = 35 ± 5.3 dB SPL) but failed to recover to BN thresholds at 24 kHz (BN = 31 ± 6.9 dB SPL, one DAN = N/A, seven DAN = 77 ± 4.9 dB SPL, 14 DAN = 60 ± 14 dB SPL).

(D) In *Nlgn1/3* dKO mice ABR thresholds fully recovered to BN threshold levels by 14 DAN at 8 kHz (BN = 35 ± 5.7 dB SPL, one DAN = 56 ± 16 dB SPL, seven DAN = 34 ± 5.3 dB SPL, 14 DAN = 60 ± 11 dB SPL) but failed to recover to BN thresholds at 16 kHz (BN = 32 ± 5.1 dB SPL, one DAN = N/A, seven DAN = N/A, 14 DAN = 76.6 ± 5.8 dB SPL) and moreover failed to generate any ABR activity above 24 kHz following noise.

(E–H) Wave I amplitudes in response to 80 dB SPL stimulation fully recovered to BN amplitudes across WT mice 14 DAN (8 kHz = 97 ± 3.4%, 16 kHz = 94 ± 8%, 24 kHz = 88 ± 5.3%). Conversely, *Nlgn1* KOs remained dramatically reduced and never recovered to baseline levels 14 DAN at 8 kHz (77 ± 11%) while *Nlgn3* KOs failed to recover at 16 and 24 kHz (16 kHz = 76 ± 7.1, 24 kHz = 26 ± 20%). *Nlgn1/3* dKOs never recovered Wave I amplitudes at any frequency compared to BN (8 kHz = 62 ± 13, 16 kHz = 19 ± 14, 24 kHz = N/A).

(I) Representative images from WT, *Nlgn1* KO, *Nlgn3* KO and *Nlgn1/3* dKO cochlear wholemounts from P60-65 mice 14 DAN, immunostained with antibodies for ribbon synapses. Scale bar = 10 μm

(J) Quantification of (I) revealed *Nlgn3* KOs and *Nlgn1/3* dKO had significantly disorganized pre- and postsynaptic elements with considerable reductions in synapse density 14 DAN (*Nlgn3* KO = 4.23 ± 14, *Nlgn1/3* dKO = 5.15 ± 1.1). Synaptic density in WT and *Nlgn1* KO cochlea had no significant difference 14 DAN.

Data are represented as mean ± SD * = p value <0.05, ** = p value <0.01, *** = p value <0.001 by one-way ANOVA with Tukey post hoc correction. N = 7 mice for (A–F), five mice for (G and H) at P60-65 per genotype.

14 DAN to determine if a reduction in synapse density underlies the weakening of Wave I response in *Nlgn3* KO (Figure 5I). On average, WT IHC contained 15 ± 0.84 ribbon synapses compared to 14 ± 0.51 ribbon synapses in *Nlgn1* KOs. Synaptic density across this region of the cochlea was significantly reduced in *Nlgn3* KOs and *Nlgn1/3 dKOs*, which on average IHCs contained only 4.2 ± 1.4 and 5.2 ± 1.1 ribbon synapses, respectively (Figure 5J). Taken together, Nlgn3 plays a far more critical role in maintaining cochlear ribbon synapse structure and function following exposure to loud noise compared to Nlgn1.

## DISCUSSION

The robust ABR phenotypes reported in the *Nlgn3* KO and *Nlgn*1/3 dKO mice manifested in the absence of a dramatic reduction of cochlear ribbon synapse density. This finding suggests that the integrity of the remaining synapses is compromised. A hypothesis supported by previous findings demonstrates that Nlgns contribute to the proper alignment of the synaptic vesicle release machinery and glutamate receptors in the CNS (Luo et al., 2021; Shipman et al., 2011). In support of this hypothesis, the distance between pre and postsynaptic elements was increased in *Nlgn1* and *Nlgn3* KO cochlea. Furthermore, AMPAR clusters were significantly enlarged in both the single and double KOs. Evidence for higher AMPAR diffusion in the absence of Nlgn1 function has been previously reported (Jeong et al., 2019; Letellier et al., 2018; Mondin et al., 2011). This displacement of AMPARs may reduce receptor density in the membrane and thus reduce synaptic strength, which may explain the ABR phenotype in the single KOs in the absence of a dramatic reduction in synapse number per IHC (Chanda et al., 2017; Luo et al., 2021; Shipman et al., 2011).

Reduced amplitude and increased latency and duration of Wave I in *Nlgn1/3* dKO mice suggest a desynchronization of SGN action potential generation, as seen in mice with deficient synaptic ribbons owing to the disruption of Bassoon or Ribeye proteins (Buran et al., 2010). Reduction in the amplitude of the excitatory postsynaptic current is expected to increase the jitter of first-spike latency in the auditory nerve (Rutherford et al., 2012), which is expected to impair aspects of sound encoding that rely on spike timing and phase locking, such as sound source localization in the horizontal plane (Rutherford et al., 2021). Reduced responses to high-intensity tones in *Nlgn3* and *Nlgn*1/3 dKO mice at baseline are expected to impair suprathreshold hearing, such as cochlear synaptopathy. Moderate noise exposure in WT mice causes a reduction in Wave I amplitude present only at higher levels of stimulation because low-threshold SGNs are largely

unaffected (Kujawa and Liberman, 2009). In contrast, the *Nlgn1/3* dKO phenotype included the reduction of Wave I amplitudes at all sound levels, suggesting the dysfunction of synapses driving both hi- and low-threshold SGNs. Additionally, *Nlgn3* KO and *Nlgn1/3* dKOs have increased sensitivity to noise exposures causing temporary threshold shifts and synaptopathy in WT mice, suggesting that ribbon synapses lacking Nlgn3 are vulnerable to prolonged, moderate noise trauma.

Our findings on the role of Nlgns in the cochlea are consistent with abundant evidence from the CNS showing that their contributions are more closely involved with the maturation rather than the development of synapses (Chanda et al., 2017; Chih et al., 2005; Jiang et al., 2017; Varoqueaux et al., 2006; Zhang et al., 2015). In the cochlea only *Nlgn3* expression consistently increased following the onset of hearing, suggesting a prominent role in the maturation of ribbon synapses (Michanski et al., 2019). In further support of Nlgn3 being a critical regulator of ribbon synapse maturation, cochlea synapse density failed to increase from P12 to P30 in *Nlgn3* KO but not *Nlgn1* KO mice. The exacerbated *Nlgn1/3* dKO phenotype compared to the single KOs, in particular *Nlgn1* KO, is consistent with previous studies (Chanda et al., 2017; Shipman et al., 2011; Zhang et al., 2017). The dramatic double KO phenotype may be owing to Nlgn1 and Nlgn3 forming heterodimers, which may modulate the affinity for binding NRXNs and function once on the surface (De Jaco et al., 2010; Poulopoulos et al., 2012; Shipman and Nicoll, 2012; Sudhof, 2008). It is important to note that ribbon synapse density in double KO at P12 was similar to WT, suggesting that other synaptic adhesion molecules (SAM) are involved and sufficient before maturation. Consistently a panel of postsynaptic SAMs including LRRTM1, LRRTM3, Flrt3, and SALM2 all of which contribute to AMPAR function in the CNS are also expressed by SGNs (de Wit et al., 2009; Nam et al., 2011; O'Sullivan et al., 2012; Shrestha et al., 2018; Soler-Llavina et al., 2011).

Mutations to *Nlgn1* and *Nlgn3* have been previously linked to autism spectrum disorder (ASD) (Guang et al., 2018; Nguyen et al., 2020; Taylor et al., 2020; Uzunova et al., 2014; Zhang et al., 2017). Given our new understanding of the role in Nlgn3 and Nlgn1 in hair cell ribbon synapse function, it is possible that altered noise sensitivity in ASD could be related to abnormalities in cochlear function or central auditory processing (Leekam et al., 2007; Miron et al., 2021). However, as Nlgn1 and Nlgn3 may function in synapses of the ascending auditory pathway, future experiments with conditional KO mice are needed to determine if these effects emanate directly from CNS deficiencies or indirectly from reduced cochlear output or both. These findings reveal novel roles for Nlgn1 and Nlgn3 in cochlear ribbon synapse structure and function, lack of which results in hearing impairment and increased vulnerability to noise trauma.

### Limitations of study

It is important to point out that our study almost exclusively relied on the use of *Nlgn1 and Nlgn3* germline gene knockout mice. In one way, this strategy was beneficial as it allowed us to study the role of neuroligins throughout cochlear development and maturation. However, it is worth pointing out that with this strategy we are unable to delineate the impact of efferent inputs on HC-SGN communication. Notably, conditional KO of *Nlgn1* recapitulated many of the phenotypes observed in the *Nlgn1* germline KO. Additionally, our functional measures of hearing relied solely on ABRs. Although convenient, this type of field recording is unable to delineate the consequence owing to the selective expression of neuroligins in individual SGNs. The use of single unit recordings would provide a more rigorous characterization of the contributions that individual neuroligins impose on cochlear ribbon synapse activity. Finally, our EM analysis lacked a large cohort of biological replicates and the spatial resolution needed to obtain a 3-dimensional ultrastructure model.

## STAR★METHODS

Detailed methods are provided in the online version of this paper and include the following:

- KEY RESOURCES TABLE
- RESOURCE AVAILABILITY
  - Lead contact
  - Materials availability
  - Data and code availability
- EXPERIMENTAL MODEL AND SUBJECT DETAILS
  - Animal experiments
- METHOD DETAILS
  - GWAS analysis

- Cochlear functional assays
- Immunofluorescence (IF)
- Quantification of synapse density, volume, and diversity
- Synapse distance quantification
- Transmission electron microscopy
- Quantification of EM images
- qPCR
- RNAScope and CellProfiler analysis
- Western Blot analysis

● QUANTIFICATION AND STATISTICAL ANALYSIS

## SUPPLEMENTAL INFORMATION

Supplemental information can be found online at https://doi.org/10.1016/j.isci.2022.104803.

## ACKNOWLEDGMENTS

We thank Joris De Wit, Jaime Garcia-Añoveros, Nopporn Jongkamonwiwat, Anis Contractor, and members of the Savas laboratory for insightful discussions. We would also like to thank Nils Brose for generously sharing Nlgn1 and Nlgn3 KO mice for this study and John Reynolds for the marmoset tissue. Some of the image analysis in this article was derived from the Northwestern University Center for Advanced Molecular Imaging, which is generously supported by NCI CCSG P30 CA060553 awarded to the Robert H Lurie Comprehensive Cancer Center. This work was supported by T32 MH067564 to M.A.R[1]., 5R01 DC018566 to R.A.F., R01 DC014712 to M.A.R.[2], R00 DC-013805, W81XWH-19-1-0627, an NU Knowles Hearing Center Pilot award to J.N.S.. U.M. is supported by the Chan-Zuckerberg Initiative Imaging Scientist Award, NSF NeuroNex Award No. 2014862, R21 DC018237, the Greenwall Foundation. The Waitt Advanced Biophotonics Core is supported by NIH-NCI CCSG: P30 014195.

## AUTHOR CONTRIBUTIONS

M.A.R[1]., M.A.R[2]., U.M., R.A.F, and J.N.S designed the experiments. M.A.R[1]. performed nearly all the experiments and S.E. participated in the proteomic analysis. Y.U. and B.O. analyzed GWAS data and performed some IF and ABRs for the cKO mice, C.M. quantified some IF. L.R.A. performed and quantified the TEM. M.A.R[1]., M.A.R[2]., and J.N.S. wrote the article.

## DECLARATION OF INTERESTS

The authors declare no competing interests.

Received: December 24, 2021
Revised: May 10, 2022
Accepted: July 15, 2022
Published: August 19, 2022

## REFERENCES

Bennett, B.J., Farber, C.R., Orozco, L., Kang, H.M., Ghazalpour, A., Siemers, N., Neubauer, M., Neuhaus, I., Yordanova, R., Guan, B., et al. (2010). A high-resolution association mapping panel for the dissection of complex traits in mice. Genome Res. *20*, 281–290. https://doi.org/10.1101/gr.099234.109.

Berg, S., Kutra, D., Kroeger, T., Straehle, C.N., Kausler, B.X., Haubold, C., Schiegg, M., Ales, J., Beier, T., Rudy, M., et al. (2019). ilastik: interactive machine learning for (bio)image analysis. Nat. Methods *16*, 1226–1232. https://doi.org/10.1038/s41592-019-0582-9.

Boussaty, E.C., Gillard, D., Lavinsky, J., Salehi, P., Wang, J., Mendonça, A., Allayee, H., Manor, U., and Friedman, R.A. (2020). The genetics of variation of the wave 1 amplitude of the mouse auditory brainstem response. J. Assoc. Res. Otolaryngol. *21*, 323–336. https://doi.org/10.1007/s10162-020-00762-3.

Budreck, E.C., and Scheiffele, P. (2007). Neuroligin-3 is a neuronal adhesion protein at GABAergic and glutamatergic synapses. Eur. J. Neurosci. *26*, 1738–1748. https://doi.org/10.1111/j.1460-9568.2007.05842.x.

Buran, B.N., Strenzke, N., Neef, A., Gundelfinger, E.D., Moser, T., and Liberman, M.C. (2010). Onset coding is degraded in auditory nerve fibers from mutant mice lacking synaptic ribbons. J. Neurosci. *30*, 7587–7597. https://doi.org/10.1523/JNEUROSCI.0389-10.2010.

Cai, T., Jen, H.I., Kang, H., Klisch, T.J., Zoghbi, H.Y., and Groves, A.K. (2015). Characterization of the transcriptome of nascent hair cells and identification of direct targets of the Atoh1 transcription factor. J. Neurosci. *35*, 5870–5883. https://doi.org/10.1523/JNEUROSCI.5083-14.2015.

Chanda, S., Hale, W.D., Zhang, B., Wernig, M., and Südhof, T.C. (2017). Unique versus redundant functions of neuroligin genes in shaping excitatory and inhibitory synapse properties. J. Neurosci. *37*, 6816–6836. https://doi.org/10.1523/JNEUROSCI.0125-17.2017.

Chih, B., Engelman, H., and Scheiffele, P. (2005). Control of excitatory and inhibitory synapse formation by neuroligins. Science *307*, 1324–1328. https://doi.org/10.1126/science.1107470.

Craig, A.M., and Kang, Y. (2007). Neurexin-neuroligin signaling in synapse development. Curr. Opin. Neurobiol. *17*, 43–52. https://doi.org/10.1016/j.conb.2007.01.011.

De Jaco, A., Lin, M.Z., Dubi, N., Comoletti, D., Miller, M.T., Camp, S., Ellisman, M., Butko, M.T., Tsien, R.Y., and Taylor, P. (2010). Neuroligin trafficking deficiencies arising from mutations in the alpha/beta-hydrolase fold protein family. J. Biol. Chem. *285*, 28674–28682. https://doi.org/10.1074/jbc.M110.139519.

de Wit, J., Sylwestrak, E., O'Sullivan, M.L., Otto, S., Tiglio, K., Savas, J.N., Yates, J.R., 3rd, Comoletti, D., Taylor, P., and Ghosh, A. (2009). LRRTM2 interacts with Neurexin1 and regulates excitatory synapse formation. Neuron *64*, 799–806. https://doi.org/10.1016/j.neuron.2009.12.019.

Furman, A.C., Kujawa, S.G., and Liberman, M.C. (2013). Noise-induced cochlear neuropathy is selective for fibers with low spontaneous rates. J. Neurophysiol. *110*, 577–586. https://doi.org/10.1152/jn.00164.2013.

Gilels, F., Paquette, S.T., Zhang, J., Rahman, I., and White, P.M. (2013). Mutation of Foxo3 causes adult onset auditory neuropathy and alters cochlear synapse architecture in mice. J. Neurosci. *33*, 18409–18424. https://doi.org/10.1523/JNEUROSCI.2529-13.2013.

Guang, S., Pang, N., Deng, X., Yang, L., He, F., Wu, L., Chen, C., Yin, F., and Peng, J. (2018). Synaptopathology involved in autism spectrum disorder. Front. Cell. Neurosci. *12*, 470. https://doi.org/10.3389/fncel.2018.00470.

Haas, K.T., Compans, B., Letellier, M., Bartol, T.M., Grillo-Bosch, D., Sejnowski, T.J., Sainlos, M., Choquet, D., Thoumine, O., and Hosy, E. (2018). Pre-post synaptic alignment through neuroligin-1 tunes synaptic transmission efficiency. Elife *7*, e31755. https://doi.org/10.7554/eLife.31755.

Hickox, A.E., Wong, A.C.Y., Pak, K., Strojny, C., Ramirez, M., Yates, J.R., 3rd, Ryan, A.F., and Savas, J.N. (2017). Global analysis of protein expression of inner ear hair cells. J. Neurosci. *37*, 1320–1339. https://doi.org/10.1523/JNEUROSCI.2267-16.2016.

Jeong, J., Pandey, S., Li, Y., Badger, J.D., 2nd, Lu, W., and Roche, K.W. (2019). PSD-95 binding dynamically regulates NLGN1 trafficking and function. Proc. Natl. Acad. Sci. USA *116*, 12035–12044. https://doi.org/10.1073/pnas.1821775116.

Jiang, M., Polepalli, J., Chen, L.Y., Zhang, B., Südhof, T.C., and Malenka, R.C. (2017). Conditional ablation of neuroligin-1 in CA1 pyramidal neurons blocks LTP by a cell-autonomous NMDA receptor-independent mechanism. Mol. Psychiatry *22*, 375–383. https://doi.org/10.1038/mp.2016.80.

Jongkamonwiwat, N., Ramirez, M.A., Edassery, S., Wong, A.C.Y., Yu, J., Abbott, T., Pak, K., Ryan, A.F., and Savas, J.N. (2020). Noise exposures causing hearing loss generate proteotoxic stress and activate the proteostasis network. Cell Rep. *33*, 108431. https://doi.org/10.1016/j.celrep.2020.108431.

Kang, H.M., Zaitlen, N.A., Wade, C.M., Kirby, A., Heckerman, D., Daly, M.J., and Eskin, E. (2008). Efficient control of population structure in model organism association mapping. Genetics *178*, 1709–1723. https://doi.org/10.1534/genetics.107.080101.

Kujawa, S.G., and Liberman, M.C. (2009). Adding insult to injury: cochlear nerve degeneration after "temporary" noise-induced hearing loss. J. Neurosci. *29*, 14077–14085. https://doi.org/10.1523/JNEUROSCI.2845-09.2009.

Leekam, S.R., Nieto, C., Libby, S.J., Wing, L., and Gould, J. (2007). Describing the sensory abnormalities of children and adults with autism. J. Autism Dev. Disord. *37*, 894–910. https://doi.org/10.1007/s10803-006-0218-7.

Letellier, M., Szíber, Z., Chamma, I., Saphy, C., Papasideri, I., Tessier, B., Sainlos, M., Czöndör, K., and Thoumine, O. (2018). A unique intracellular tyrosine in neuroligin-1 regulates AMPA receptor recruitment during synapse differentiation and potentiation. Nat. Commun. *9*, 3979. https://doi.org/10.1038/s41467-018-06220-2.

Liberman, M.C. (1982). Single-neuron labeling in the cat auditory nerve. Science *216*, 1239–1241.

Luo, J.K., Melland, H., Nithianantharajah, J., and Gordon, S.L. (2021). Postsynaptic neuroligin-1 mediates presynaptic endocytosis during neuronal activity. Front. Mol. Neurosci. *14*, 744845. https://doi.org/10.3389/fnmol.2021.744845.

Lusis, A.J., Seldin, M.M., Allayee, H., Bennett, B.J., Civelek, M., Davis, R.C., Eskin, E., Farber, C.R., Hui, S., Mehrabian, M., et al. (2016). The Hybrid Mouse Diversity Panel: a resource for systems genetics analyses of metabolic and cardiovascular traits. J. Lipid Res. *57*, 925–942. https://doi.org/10.1194/jlr.R066944.

Meyer, A.C., Frank, T., Khimich, D., Hoch, G., Riedel, D., Chapochnikov, N.M., Yarin, Y.M., Harke, B., Hell, S.W., Egner, A., and Moser, T. (2009). Tuning of synapse number, structure and function in the cochlea. Nat. Neurosci. *12*, 444–453. https://doi.org/10.1038/nn.2293.

Michanski, S., Smaluch, K., Steyer, A.M., Chakrabarti, R., Setz, C., Oestreicher, D., Fischer, C., Möbius, W., Moser, T., Vogl, C., and Wichmann, C. (2019). Mapping developmental maturation of inner hair cell ribbon synapses in the apical mouse cochlea. Proc. Natl. Acad. Sci. USA *116*, 6415–6424. https://doi.org/10.1073/pnas.1812029116.

Miron, O., Delgado, R.E., Delgado, C.F., Simpson, E.A., Yu, K.H., Gutierrez, A., Zeng, G., Gerstenberger, J.N., and Kohane, I.S. (2021). Prolonged auditory brainstem response in universal hearing screening of newborns with autism spectrum disorder. Autism Res. *14*, 46–52. https://doi.org/10.1002/aur.2422.

Mondin, M., Labrousse, V., Hosy, E., Heine, M., Tessier, B., Levet, F., Poujol, C., Blanchet, C., Choquet, D., and Thoumine, O. (2011). Neurexin-neuroligin adhesions capture surface-diffusing AMPA receptors through PSD-95 scaffolds. J. Neurosci. *31*, 13500–13515. https://doi.org/10.1523/JNEUROSCI.6439-10.2011.

Nam, J., Mah, W., and Kim, E. (2011). The SALM/Lrfn family of leucine-rich repeat-containing cell adhesion molecules. Semin. Cell Dev. Biol. *22*, 492–498. https://doi.org/10.1016/j.semcdb.2011.06.005.

Nguyen, T.A., Lehr, A.W., and Roche, K.W. (2020). Neuroligins and neurodevelopmental disorders: X-linked genetics. Front. Synaptic Neurosci. *12*, 33. https://doi.org/10.3389/fnsyn.2020.00033.

O'Sullivan, M.L., de Wit, J., Savas, J.N., Comoletti, D., Otto-Hitt, S., Yates, J.R., 3rd, and Ghosh, A. (2012). FLRT proteins are endogenous latrophilin ligands and regulate excitatory synapse development. Neuron *73*, 903–910. https://doi.org/10.1016/j.neuron.2012.01.018.

Petitpré, C., Wu, H., Sharma, A., Tokarska, A., Fontanet, P., Wang, Y., Helmbacher, F., Yackle, K., Silberberg, G., Hadjab, S., and Lallemend, F. (2018). Neuronal heterogeneity and stereotyped connectivity in the auditory afferent system. Nat. Commun. *9*, 3691. https://doi.org/10.1038/s41467-018-06033-3.

Poulopoulos, A., Soykan, T., Tuffy, L.P., Hammer, M., Varoqueaux, F., and Brose, N. (2012). Homodimerization and isoform-specific heterodimerization of neuroligins. Biochem. J. *446*, 321–330. https://doi.org/10.1042/BJ20120808.

Rutherford, M.A., Chapochnikov, N.M., and Moser, T. (2012). Spike encoding of neurotransmitter release timing by spiral ganglion neurons of the cochlea. J. Neurosci. *32*, 4773–4789. https://doi.org/10.1523/JNEUROSCI.4511-11.2012.

Rutherford, M.A., von Gersdorff, H., and Goutman, J.D. (2021). Encoding sound in the cochlea: from receptor potential to afferent discharge. J. Physiol. *599*, 2527–2557. https://doi.org/10.1113/JP279189.

Scheffer, D.I., Shen, J., Corey, D.P., and Chen, Z.Y. (2015). Gene expression by mouse inner ear hair cells during development. J. Neurosci. *35*, 6366–6380. https://doi.org/10.1523/JNEUROSCI.5126-14.2015.

Scheiffele, P., Fan, J., Choih, J., Fetter, R., and Serafini, T. (2000). Neuroligin expressed in nonneuronal cells triggers presynaptic development in contacting axons. Cell *101*, 657–669. https://doi.org/10.1016/s0092-8674(00)80877-6.

Shipman, S.L., and Nicoll, R.A. (2012). Dimerization of postsynaptic neuroligin drives synaptic assembly via transsynaptic clustering of neurexin. Proc. Natl. Acad. Sci. USA *109*, 19432–19437. https://doi.org/10.1073/pnas.1217633109.

Shipman, S.L., Schnell, E., Hirai, T., Chen, B.S., Roche, K.W., and Nicoll, R.A. (2011). Functional dependence of neuroligin on a new non-PDZ intracellular domain. Nat. Neurosci. *14*, 718–726. https://doi.org/10.1038/nn.2825.

Shrestha, B.R., Chia, C., Wu, L., Kujawa, S.G., Liberman, M.C., and Goodrich, L.V. (2018). Sensory neuron diversity in the inner ear is shaped by activity. Cell *174*, 1229–1246.e17. https://doi.org/10.1016/j.cell.2018.07.007.

Soler-Llavina, G.J., Fuccillo, M.V., Ko, J., Südhof, T.C., and Malenka, R.C. (2011). The neurexin ligands, neuroligins and leucine-rich repeat transmembrane proteins, perform convergent

and divergent synaptic functions in vivo. Proc. Natl. Acad. Sci. USA *108*, 16502–16509. https://doi.org/10.1073/pnas.1114028108.

Song, J.Y., Ichtchenko, K., Südhof, T.C., and Brose, N. (1999). Neuroligin 1 is a postsynaptic cell-adhesion molecule of excitatory synapses. Proc. Natl. Acad. Sci. USA *96*, 1100–1105. https://doi.org/10.1073/pnas.96.3.1100.

Südhof, T.C. (2008). Neuroligins and neurexins link synaptic function to cognitive disease. Nature *455*, 903–911. https://doi.org/10.1038/nature07456.

Südhof, T.C. (2017). Synaptic neurexin complexes: a molecular code for the logic of neural circuits. Cell *171*, 745–769. https://doi.org/10.1016/j.cell.2017.10.024.

Sun, S., Babola, T., Pregernig, G., So, K.S., Nguyen, M., Su, S.S.M., Palermo, A.T., Bergles, D.E., Burns, J.C., and Müller, U. (2018). Hair cell mechanotransduction regulates spontaneous activity and spiral ganglion subtype specification in the auditory system. Cell *174*, 1247–1263.e15. https://doi.org/10.1016/j.cell.2018.07.008.

Takahashi, S., Sun, W., Zhou, Y., Homma, K., Kachar, B., Cheatham, M.A., and Zheng, J. (2018). Prestin contributes to membrane compartmentalization and is required for normal innervation of outer hair cells. Front. Cell. Neurosci. *12*, 211. https://doi.org/10.3389/fncel.2018.00211.

Taylor, S.C., Ferri, S.L., Grewal, M., Smernoff, Z., Bucan, M., Weiner, J.A., Abel, T., and Brodkin, E.S. (2020). The role of synaptic cell adhesion molecules and associated scaffolding proteins in social affiliative behaviors. Biol. Psychiatry *88*, 442–451. https://doi.org/10.1016/j.biopsych.2020.02.012.

Uzunova, G., Hollander, E., and Shepherd, J. (2014). The role of ionotropic glutamate receptors in childhood neurodevelopmental disorders: autism spectrum disorders and fragile x syndrome. Curr. Neuropharmacol. *12*, 71–98. https://doi.org/10.2174/1570159X113116660046.

van Nas, A., Ingram-Drake, L., Sinsheimer, J.S., Wang, S.S., Schadt, E.E., Drake, T., and Lusis, A.J. (2010). Expression quantitative trait loci: replication, tissue- and sex-specificity in mice. Genetics *185*, 1059–1068. https://doi.org/10.1534/genetics.110.116087.

Varoqueaux, F., Aramuni, G., Rawson, R.L., Mohrmann, R., Missler, M., Gottmann, K., Zhang, W., Südhof, T.C., and Brose, N. (2006). Neuroligins determine synapse maturation and function. Neuron *51*, 741–754. https://doi.org/10.1016/j.neuron.2006.09.003.

Yin, Y., Liberman, L.D., Maison, S.F., and Liberman, M.C. (2014). Olivocochlear innervation maintains the normal modiolar-pillar and habenular-cuticular gradients in cochlear synaptic morphology. J. Assoc. Res. Otolaryngol. *15*, 571–583. https://doi.org/10.1007/s10162-014-0462-z.

Zhang, B., Chen, L.Y., Liu, X., Maxeiner, S., Lee, S.J., Gokce, O., and Südhof, T.C. (2015). Neuroligins sculpt cerebellar purkinje-cell circuits by differential control of distinct classes of synapses. Neuron *87*, 781–796. https://doi.org/10.1016/j.neuron.2015.07.020.

Zhang, B., Seigneur, E., Wei, P., Gokce, O., Morgan, J., and Südhof, T.C. (2017). Developmental plasticity shapes synaptic phenotypes of autism-associated neuroligin-3 mutations in the calyx of Held. Mol. Psychiatry *22*, 1483–1491. https://doi.org/10.1038/mp.2016.157.

## STAR★METHODS

### KEY RESOURCES TABLE

| REAGENT or RESOURCE | SOURCE | IDENTIFIER |
|---|---|---|
| Antibodies | | |
| GAPDH | Abcam | Cat# ab181602; RRID: AB_2630358 |
| CtBP2 | BD Transduction Laboratories | Cat# 612,044; RRID: AB_399431 |
| GluA2 | Millipore | Cat# MAB397; RRID: AB_2113875 |
| Nlgn1 | R&D Systems | Cat# AF4340; RRID: AB_2151652 |
| Nlgn2 | Invitrogen | Cat# PA5-77523; RRID: AB_2736214 |
| Nlgn3 | Novus | Cat# NBP1-90080; RRID: AB_11027178 |
| Pan-NRXN | Synaptic Systems | Cat# 175,003; RRID: AB_10697815 |
| Syt1 | Synaptic Systems | Cat# 105,011; RRID: AB_2619760 |
| Neurofilament H | Synaptic Systems | Cat# 171,106; RRID: AB_2721078 |
| Critical commercial assays | | |
| NEBNext® UltraTM RNA Library Prep Kit | New England Bio Labs | Cat# E7770 |
| RNAscope® Multiplex Fluorescent Reagent Kit V2 | ACD | Cat# 323,100 |
| TRIzol | Invitrogen | Cat# 15,596,026 |
| RNeasy Mini Kit | Qiagen | Cat# 74,106 |
| iScript™ cDNA Synthesis kit | BioRad | Cat# 1,708,890 |
| Power SYBR™ Green PCR Master Mix | Applied Biosystems | Cat# 43-676-59 |
| Experimental models: Organisms/strains | | |
| $B_6$; 129-Nlgn1tm1Bros/J | Jax | Stock No: 008136 |
| B6-Nlgn3tmBros | Nils Brose | N/A |
| Oligonucleotides | | |
| Nlgn1-Forward ACCATGGCACTTCCCAGATG | This Paper | N/A |
| Nlgn1-Reverse AAGCAGAGAGTCAATGGGGC | This Paper | N/A |
| Nlgn2-Forward CCACTCAGAAGGACTGTTCC | This Paper | N/A |
| Nlgn2-Reverse CTGTCTTCTCGGTCACAGC | This Paper | N/A |
| Nlgn3-Forward ATCGGTGCATCCTGTGTCAG | This Paper | N/A |
| Nlgn3-Reverse ATCGGTGCATCCTGTGTCAG | This Paper | N/A |
| NEUN-Forward CCACTCTCTTGTCCGTTTGC | This Paper | N/A |
| NEUN-Reverse TCTGTAAGCTGCATAGCCTCC | This Paper | N/A |
| Software and algorithms | | |
| RStudio | CRAN R Project | Version 1.3.959 |
| Graphpad | Graphpad | Version 8.4.3, RRID: SCR_002798 |
| PicoLog system | PCP Piezotronic | Picoscope 2000 series |
| BioSigRP | Tucker Davis Technologies | Version 4.4, RRID: SCR_006495, |
| Matlab | MathWorks | R2019b, RRID: SCR_001622 |
| Other | | |
| Mm-Nlgn1-02-C2 | ACD | Cat# 894021-C2 |
| Mm-Nlgn3-01-C1 | ACD | Cat# 513541 |
| Tubb3-C3 | ACD | Cat# 423391-C3 |
| Myo7a-C3 | ACD | Cat# 462771-C3 |
| Speaker compression driver | JBL | Cat# 2446H/J |
| DPOAE Speakers | Etymotic | Cat# ER10B$^+$ |

(*Continued on next page*)

*Continued*

| REAGENT or RESOURCE | SOURCE | IDENTIFIER |
|---|---|---|
| Soundproof chamber | EcKel Audiometric | N/A |
| Genuine grass platinum subdermal needle electrode | Natus Neurology | Cat# F-E2-24 |
| ABR and DPOAE system | Tucker-Davis Technologies | RRID: SCR_006495, RZ6 Multi I/O Processor |
| Precellys 24 | Bertin Technology | N/A |
| ACD HybEZTM II Hybridization System (110v) | ACD | Cat# 321710 |
| NanoPhotometer® spectrophotometer | IMPLEN | N/A |
| StepOnePlus Real-ime PCR System | ThermoFisher | Cat# 4376600 |
| MATLAB CODE | Zenodo | Zenodo: 510823728, https://zenodo.org/badge/latestdoi/510823728 |

## RESOURCE AVAILABILITY

### Lead contact

Further information and requests for resources and reagents should be directed to and will be fulfilled by the lead contact, Jeffrey N. Savas (jeffrey.savas@northwestern.edu).

### Materials availability

This study did not generate new unique reagents.

### Data and code availability

- Microscope data reported in this paper will be shared by the lead contact upon request.
- Matlab code is available from: Zenodo: 510823728, https://zenodo.org/badge/latestdoi/510823728
- Any additional information required to reanalyze the data reported in this paper is available from the lead contact upon request.

## EXPERIMENTAL MODEL AND SUBJECT DETAILS

### Animal experiments

All animal experiments were conducted according to Northwestern University Institutional Animal Care and Use Committee (IACUC), Northwestern University IACUC (approved protocol numbers IS00001182). For euthanasia, pups were immediately decapitated, and adult animals were euthanized by isoflurane overdose and decapitation. In all studies, mice of both sexes were used in similar number, however our study was not sufficiently powered in order to determine sex specific effect. The Institutional Care and Use Committee (IACUC) at University of California San Diego (IACUC 17178) and University of Southern California (IACUC 12033) endorsed the animal protocol for the Hybrid Mouse Diversity Panel (HMDP) inbred strains. Strains and genotypes are accessible from the Jackson Laboratories (www.jax.org). Dr. John Reynolds (Salk Institute) generously donated marmoset tissues. All results required to corroborate the conclusions presented here are provided entirely within this article.

## METHOD DETAILS

### GWAS analysis

GWAS for ABR Wave I amplitude in the HMDP (Bennett et al., 2010), were performed, as described previously (Boussaty et al., 2020). Briefly, five-week-old female mice (n = 635) from 102 HMDP strains (n = 6-7 strains/strain) underwent ABR analysis, and peak to peak (P1-N1) values for Wave I amplitudes with 80 dB SPL stimuli at 8, 16, 24 and 32 kHz were measured and utilized for the GWAS study. The phenotypes in the HMDP strains were managed using genotypes of 500,000 single nucleotide polymorphisms (SNPs) obtained from the Mouse Diversity Array (minor allele frequencies >5%; missing genotype frequencies <10%) (van Nas et al., 2010). FaST-LMM (factored spectrally transformed linear mixed model) was utilized to analyze the GWAS, and 100 different sets of permutation tests and parametric bootstrapping of size 1000 was performed. The genome-wide significance threshold at a family-wise error rate (FWER) of 0.05 corresponded to $p = 4.1 \times 10^{-6}$ was observed, similar to that used in previous studies with the HMDP (Bennett et al., 2010). For prioritizing candidate genes, EMMA (Efficient Mixed-Model Association) was utilized

for performing an association between all SNPs and array probes mapping within each region (Kang et al., 2008). Additional analyses were performed using Locus zoom for displaying the linkage disequilibrium (LD). RefSeq genes were downloaded from the UCSC genome browser (https://genome.ucsc.edu/cgi-bin/hgTracks?db=mm10) using the GRCm38/mm10 genome assembly to characterize the genes located within each association.

### Cochlear functional assays

Auditory brainstem responses (ABRs) and distortion product otoacoustic emission (DPOAE) were recorded in young adult mice (P60-65). ABR and DPOAE recordings were obtained by Tucker Davis Technologies (TDT) System III workstation running BioSigRP in a soundproof chamber (EcKel audiometric room, Cambridge, MA). ABR stimuli were pre-amplified with a 4-channel MEDUSA pre-amp and analyzed by a real-time processor in TDT system3. Prior to electrode placement, animals were anesthetized by intraperitoneal injection of Ketamine and Xylazine cocktails given at a dose of 100 mg/kg and 3 mg/kg body weight, respectively. The top-up injections (quarter of the original dose) were administered as needed. Animal body temperature was maintained at 37–38 °C by electric heating pad (Homeothermic blanket system, Harvard Apparatus). Subcutaneous platinum needle electrodes were placed at the vertex (recording) and ipsilateral mastoid (reference), with the ground electrode placed on the lower back. ABRs were measured in response to 20-millisecond tone pips, ranging from 8-28 kHz in 4 kHz increments and from 10 to 80 dB SPL in 5 dB steps from 10 to 40 dB and 10 dB steps from 40 to 80 dB SPL. The average response to 500 tone pips was displayed on a PC monitor during the experiments using operating software (BioSigRP, TDT). ABR thresholds were defined as the lowest stimulus level (dB SPL) for which a recognizable ABR wave I was measured with an amplitude 0.18 μVs above the noise floor. The amplitude of ABR Wave-I was estimated by measuring the voltage difference between the Wave-I peak (P1) and the trough between Wave-I and wave-II (N1). Similarly, the duration of wave-I was measured as the time between P1 and N1. DPOAE recording was verified by using Etymotic low noise microphone system ER-10B+. The stimulus consists of two primary pure-tone frequencies ($f_1$ and $f_2$) differing by a factor of 1.2. The $L_1$ and $L_2$ values were varied from 15 to 75 dB SPL ($L_1 > L_2$, 5 dB) in 5 dB step across the frequency from 8-32 kHz. The spectral magnitude of the two primaries, $2f_1 - f_2$ distortion product, and the noise floor will be determined from an averaging of 500 stimuli.

Noise exposures were delivered to unanesthetized animals held within small wire cages in a custom-built sound-proof chamber designed by Charles Liberman (Mass. Eye and Ear). The box is constructed of 3/4″ plywood sheets. The basic principle is that no two sides are parallel. The front and back panel are the same, except that the back is truncated at a height of 42′′ (rather than 48″) and has no door. This makes the top slanted with respect to the floor. The side panels are then cut to fit. The top panel has a rectangular hole cut in it to which an exponential horn and the acoustic driver are mounted.

Waveforms used for acoustic overexposure were designed using a waveform generator (Tucker-Davis Technologies, Alachua, FL) within the frequency range of 8–16 kHz for 30 min. Noise level intensity was delivered through an exponential horn extending from compression driver (JBL, 2446H/J, Northridge, CA). Mice were exposed to 94 dB SPL (1.00 Pa SIL) Noise generation stability was monitor by PicoLog system (Picoscope 2000 series) and calibrating microphone (PCP Piezotronics, NY).

### Immunofluorescence (IF)

Mice were sacrificed and temporal bones were isolated in less than ten minutes after euthanasia. Samples were then rinsed in ice-cold PBS amended with Halt protease inhibitor cocktail until buffer remained clear of blood following vortexing. Oval and round windows were punctured, and a small hole was created near the apex of the cochlea to gently perfuse the scalae with PKS solution (4% paraformaldehyde, 126 mM NaCl, 2.5 mM KCl, 25 mM $NaHCO_3$, 1.2 mM $NaH_2PO_4$, 1.2 mM $MgCl_2$, 2.5 mM $CaCl_2$, 11 mM sucrose), followed by bath fixation in PKS for 1 hour at 4 °C. Cochleae were decalcified in Immunocal (Decal Chemical Corporation, Congers, NY) for two hours at 4 °C or until cochleae became translucent. The decalcified bone, lateral wall, Reissner's membrane, and tectorial membranes were dissected away from the organ of Corti. For whole mount preparation, cochleae were then divided into 4 pieces and cryoprotected in 30% sucrose for 30 minutes prior to freezing on dry ice. The frozen pieces were then thawed and rinsed three times in PBS for 10 minutes at room temperature with agitation. Cochlear pieces were then blocked overnight in 20% normal horse serum with 1% Triton-X blocking buffer at 4 °C. Primary antibodies were diluted in blocking buffer as follows: Recombinant Neurofilament H (1:1000), CtBP2 (1:200), GluA2

(1:100), Nlgn1 (1:100), Nlgn2 (1:100), Nlgn3 (1:100), Syt1 (1:300), and Pan-NRXN (1:100) prior to being incubated at 37 °C overnight. Following primary antibody incubation pieces were rinsed three times with PBS for 15 minutes at room temperature. Pieces were then incubated in secondary antibody: Goat Anti-Mouse IgG2a (1:500, Alexa Fluor 488, Abcam, A21131), Goat Anti-Mouse IgG1 (1:500, Alexa Fluor 568, Abcam, A21124), Goat Anti-Rabbit H&L (1:250, Alexa Fluor 647, Abcam, A27040), Donkey Anti-Sheep H&L (1:250, Alexa Fluor 647, Abcam, ab150179), Donkey Anti-Sheep H&L (1:250, Alexa Fluor 405, Abcam, ab175676) for three hours at room temperature. Samples were then rinsed three times in PBS for 15 minutes and stained with DAPI Staining Solution (Abcam, ab228549) for 5 minutes prior to mounting in ProLong Gold Antifade Mountant (Thermo Scientific, cat. P10144). Images were captured with confocal laser scanning microscopy (Leica DMI4000) with identical settings.

Marmoset monkey (61 months old) was euthanized due to an emergency health condition with a lethal dose of Euthasol (200 mg/kg IP). Temporal bones were harvested and stored in 4% paraformaldehyde until histological analysis. The temporal bone and cochlea were skeletonized by using an electrical drill (4300; DREMELL, Illinois U.S.), then membranous labyrinth was carefully taken out by 3 pieces: apical, middle and basal turn. Each cochlear turn was divided into 4 to 5 pieces. Cochlear samples were permeabilized in PBS with 0.3% triton X (TX) and blocked with 5% normal goat serum (NGS) for 30 min at room temperature. Samples were incubated with primary antibodies, CtBP2 (1:200) and Nlgn1(1:100), in PBS and 0.03% TX with 3% NGS at 37 °C overnight, followed by secondary antibodies for 30 min at room temperature. Images were taken with a confocal laser scanning microscope (LSM880; Carl Zeiss, Jena, Germany) with Airyscan processing.

### Quantification of synapse density, volume, and diversity

Synaptic coordinates and volumes were obtained from confocal stacks after deconvolution with the AMIRA FEI software suite and processing in MATLAB. Images were imported into AMIRA and islands larger than 5 pixels were removed prior to analysis. Synaptic volumes were acquired by measuring the intersection of CtBP2 and GluA2 puncta in 3-demenstional space. 3D image analysis recorded coordinates of ribbon puncta (anti-CtBP2) overlaid onto either anti-Nlgn1 or anti-Nlgn3 puncta which were then rotated using matrix transformation and centered onto the zero coordinate to orient all data points onto the same plane, only data for paired structures is presented. To obtain positional information for paired ribbon synapses, we adapted methods previously described (Gilels et al., 2013; Yin et al., 2014). In brief, to analyze the distribution of synapses along the pillar-modiolar axis, rotated datasets were oriented into a cross-sectional quadrant plane representing the pillar-modiolar axis (x-axis) and basal-apical axis (z-axis) in MATLAB (N = 5 mice, 75 IHCs, 1306 synapses). The midpoints of both axes for each tissue sample were aligned to normalize these positions with the other data stacks of the same genotype before analysis. The population clusters were chosen using the implemented Bayesian information criterion and were constrained to the 90% quantile with two possible population clusters for each dataset. Synapses containing only Nlgn1, only Nlgn3, or both neuroligins were then segregated and plotted for visual comparison of spatial distributions along the pillar to modiolar face of the IHC. Synapses were then divided into pillar and modiolar groups based on their distance from the center point of the Z axis for comparison of spatial distributions of Nlgn1 and Nlgn3. Percentages were taken as the proportion of synapses for each group (i.e. Nlgn1 only) on either the pillar or modiolar face over the total measured synapses for that group.

### Synapse distance quantification

For each image of synapse markers CtBP2 and GluA2, the two channels were separated and segmented individually using Ilastik pixel classification (Berg et al., 2019), yielding a three-dimensional segmentation of each. Within each channel, the intensity-weighted centroids of each segmented object were first found, and then the centroid-to-centroid distances between all possible CtBP2 and GluA2 pairs were calculated. For each CtBP2 punctum, the nearest GluA2 punctum was identified. The opposite was also done, generating a list the nearest CtBP2 punctum to each GluA2 punctum. Only puncta paired as nearest neighbors on both lists were classified as paired synapses. Pairs existing on only one list were discarded as mismatched lone puncta (Figure 3H).

### Transmission electron microscopy

Following sedation animals were perfused via peristaltic pump at a rate of 0.72 mL/min of fixation solution (2.5% glutaraldehyde, 4% paraformaldehyde, 0.1 M sodium cacodylate, 5 mM CaCl2, and 2 mM MgCl2) for 10 mins through the heart. Inner ears were then harvested from the brain cavity, both oval and round

windows were perforated in addition to a small incision near the apex of the cochlea prior to overnight incubation in a new bath of fixative at 4°C. Next, samples were washed in PBS (3 × 15 min), the cochleae fine dissected and transferred to glass vials for post-fixation with 1% osmium tetroxide and 1.2% potassium ferricyanide in 0.1 M sodium cacodylate buffer (reduced osmium) for 40 min RT, washed 3 times in buffer, stained with 1% uranyl acetate for 1 h, dehydrated in graded acetone dilutions till absolute, embedded with Epon resin and polymerized for 2 days at 60 °C. Sections of 70-nm thickness were cut (Leica UC7 ultramicrotome) and transferred to silicon chips (University Wafer Inc.). Cells were then imaged using a Zeiss Sigma VP operated at 3 kV, collecting back-scattered electrons images with 2nm-pixel size of resolution. All chemical reagents were bought from Electron Microscopy Sciences (EMS).

### Quantification of EM images

We defined two parameters to quantify: the distance between the inner hair cell membrane and the neuronal membrane (synaptic cleft), and the angle of the rod of the ribbon synapse with respect to the IHC membrane. ImageJ Fiji (NIH) was used to quantitate the images acquired via EM, a total of 2 animals per group, 6 cells per condition and at least 25 synapses in total were quantified. After calibration of the pixel size within the software, orthogonal lines were traced in different regions (2–5) along the length of the membrane closest to the cochlear ribbon. The average of these measurements was then taken as the distance between the pre and postsynaptic membranes of the cochlear ribbon synapse cleft.

### qPCR

RNA was isolated from dissected cochleae of postnatal day 1 (P1), P6, P12, P30 and P60 mice using TRIzol and RNeasy Kit (Qiagen). RNA was reverse transcribed using iScript cDNA Synthesis kit (Bio-Rad). Real-time PCR was performed with StepOnePlus Real-Time PCR system (Applied Biosystems) using Power SYBR Green Master Mix (Applied Biosystems). A total of 50 ng of cDNA was used for each reaction. Cycling parameters were as follows: 95 °C for 10 min; 40 cycles of 95 °C for 15 s, and 60 °C for 60 s. A minimum of five biological replicates were used for each target. Primers were sourced from Qiagen (QuanTitect primer assays) and were reconstituted to 10μM concentrations. All datasets were normalized to individual *NeuN* CT values to measure differences in neuronal RNA prior to comparison to WT gene expression levels.

### RNAScope and CellProfiler analysis

Mouse cochleae were harvested and dissected as described above. Cochlea were fixed for 1 hour then decalcified with Immunocal O/N prior to cryoprotection O/N in 30% sucrose buffer. Once saturated, cochlea were mounted in OCT and frozen O/N at −80 °C. Cochlea were then sectioned in 12 μm slices and mounted onto frosted glass slides and stored at −80 °C. Slides were washed 3 times in PBS at room temperature then sequentially dehydrated with 30%, 50%, 70%, and 100% EtOH at room temperature. Slides were then incubated in 3% hydrogen peroxide at room temperature for 10 min. Then treated with RNAscope Protease III for 15 min at 40 °C prior to rinsing three times in DEPC treated water. RNAScope probes were prewarmed at 40°C in the water bath for 10 min to dissolve precipitation. Afterwards the probes were cool down to room temperature prior to mixing the target probes of C1, C2, and C3 in a 1.5 mL tube in a 50:1:1 ratio with a final volume of 50 μL per sample. Slides were then incubated with probe mix solution at 40°C for 2 hours in the HybEZ Oven. Each channel was then amplified and hybridized to a fluorophore per manufacturer's instructions prior to staining with DAPI. Images were captured with confocal laser scanning microscopy (Leica DMI4000) with identical settings.

The maximum-intensity projection from each image stack was then filtered to remove any nuclei smaller than 7 μm in diameter or had a width that was less than a third of its length to remove supporting cells within the spiral ganglion from analysis. Resulting images were then imported into CellProfiler for further processing. Important steps in our pipeline identified the outlines of each nucleus and expanded this area 10 pixels in each direction to represent the area of the cell body. *Nlgn1* and *Nlgn3* were then independently overlaid onto the cell mask regions to determine cells which express either *Nlgn1* or *Nlgn3*. Sequential masks were then created to determine which cells express both neuroligins and which cells express only *Nlgn1* or *Nlgn3*.

### Western Blot analysis

Brains were rinsed in PBS prior to homogenization in Syn-PER buffer (Thermo Scientific, cat. 87793) amended with 1% Triton-X (Sigma-Aldrich, cat. T8787) and 0.5% SDS by Percellys 24 (Bertin, cat.

P000669-PR240-A) with three 30 second pulses at 6800 rpm at room temperature. Lysates were then incubated on ice for 10 minutes prior to needle sonication, QSonica Q700 Sonicator (M2 Scientifics, cat Q700), with amplitude set to 20 for 30 seconds. Lysates were then incubated on ice for 30 minutes, followed by centrifugation for 5 minutes at 10,000 X G at 4 °C. Supernatants were collected, and protein concentrations were measured with Pierce BCA protein assay (Thermo Scientific, cat. 23225). Twenty-five micrograms of cochlear lysates were then amended with 6X Loading Buffer and boiled at 100 °C for 5 minutes and immediately run on 10% Tris gel (Bio-Rad) and transferred to nitrocellulose membrane using Bio-Rad Trans-Blot Turbo transfer system (1.3A −25V-10 minute). Membranes were blocked with 1X Odyssey blocking solution (LI-COR, 927–70001) for one hour at room temperature and incubated with primary antibody (1:1000) overnight at 4 °C. Membranes were washed three times with TBST and incubated with secondary antibodies for two hours at room temperature. Blots were then images on the Odyssey DLx Imager.

## QUANTIFICATION AND STATISTICAL ANALYSIS

Statistical analyses were performed using Excel (Microsoft, Seattle, WA) and MATLAB. All values in figures with error bars are presented as mean ± SD. Tests with multiple measures for each stimuli intensity or frequency across all four genotypes (i.e. ABR thresholds, DPOAE thresholds, and wave I amplitude), were compared by one-way ANOVA, comparative p-values between genotypes were adjusted to correct for multiple comparisons using Tukey's method. An adjusted p-value of $<0.05$ was set as the threshold for statistical significance. Measured synapse volumes were normalized to the median value recorded in each respective image dataset and tested for the probability of Gaussian or log normal distributions. Outliers were then identified utilizing the ROUT method in Prism based on linear regression with a false discovery rate (FDR) of 1% in each respective dataset prior to analysis by one-way ANOVA with Benjamini-Hochberg correction of 0.01. Synaptic distances were quantified via Welch's t-test and an adjusted p-value of $<0.05$ was set as the threshold for statistical significance.